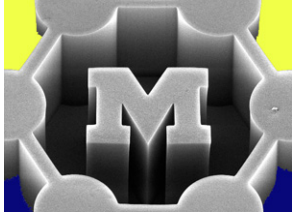

22: Balancing interactions in self-assembly and nanomanufacturing

April 14, 2010

John Hart
ajohnh@umich.edu
http://www.umich.edu/~ajohnh

Announcements

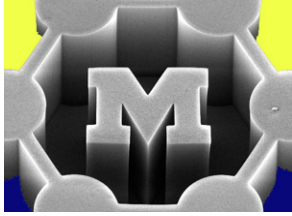

- Project presentations next M, 6-9pm, 165 CC
- Project reports due Tues (Apr/20) 5pm; may be submitted as late as Fri (Apr/**23**) without penalty

Recap: networks

- Electrical
  - Percolation theory: sudden onset of conductive behavior
  - Geometry of conductors determines percolation threshold
  - Geometry and conductivities determine scaling behavior

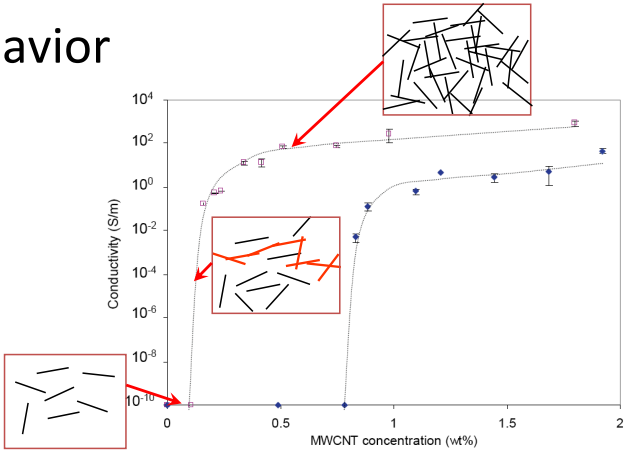

- Thermal
  - Phonon scattering at interfaces dominates

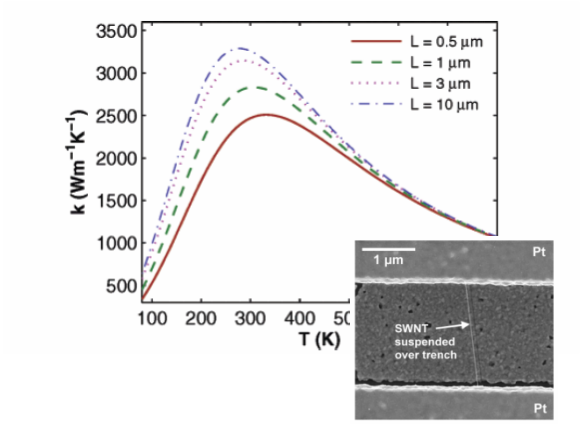

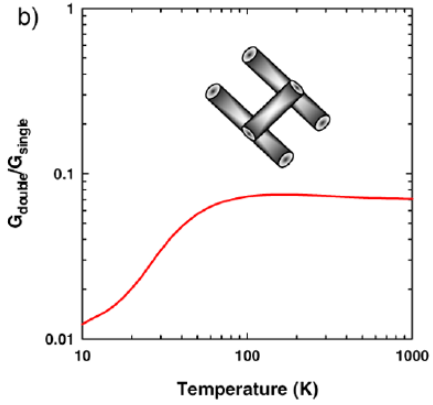

- Mechanical
  - Only direct contact matters
  - Interfaces determine load transfer
  - Joints and defects limit strength

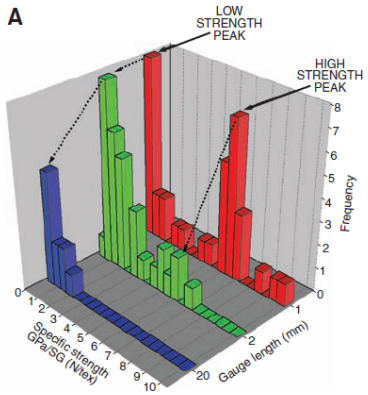

Electrical properties of CNT assemblies

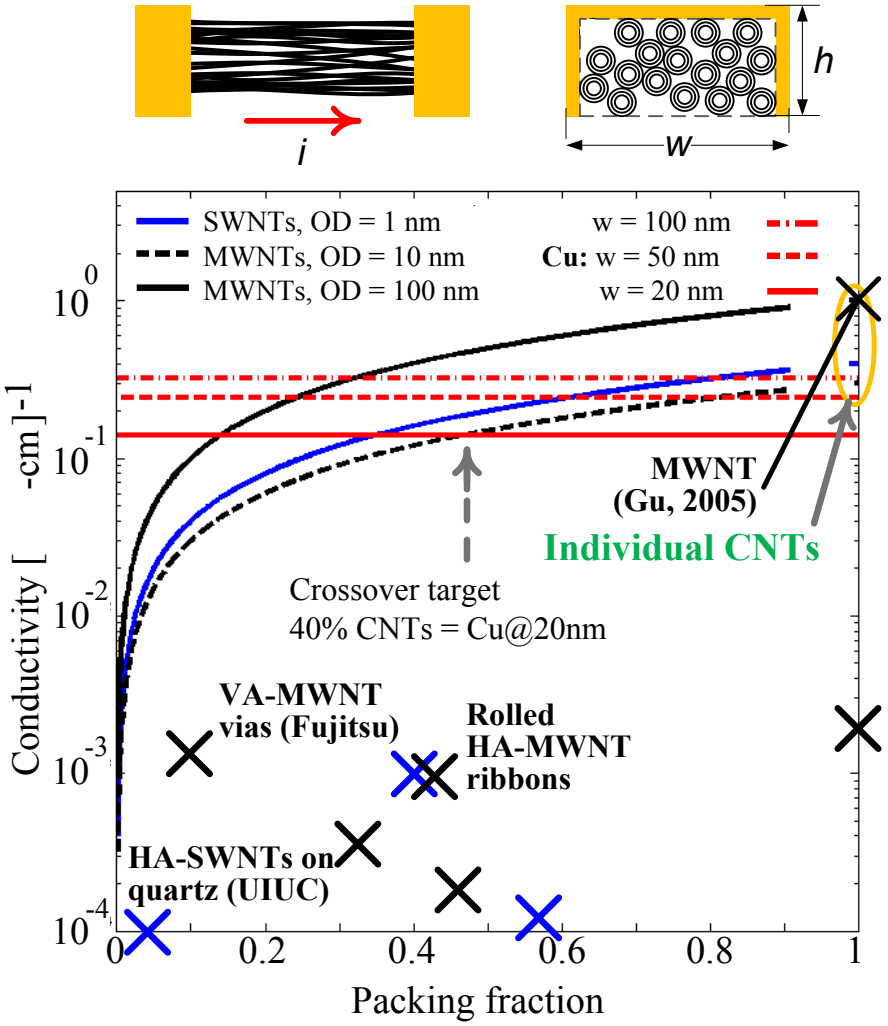

Mechanical properties of CNT assemblies

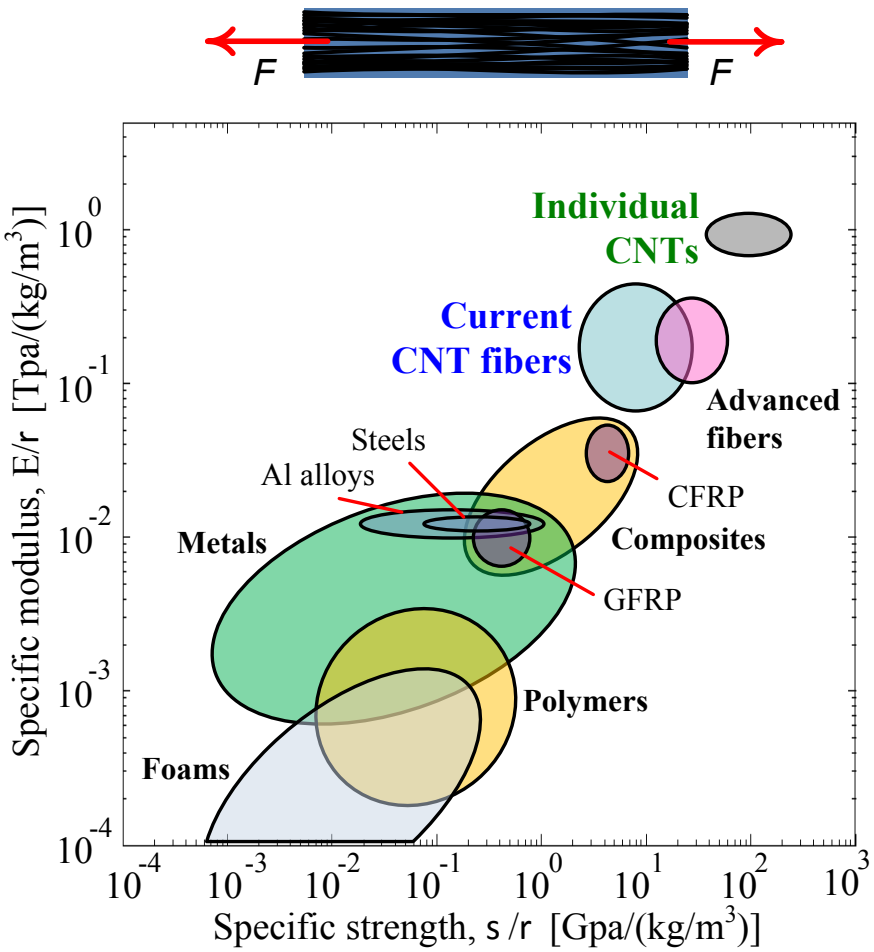

Today's agenda

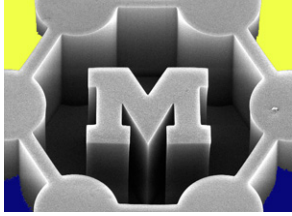

- By way of case studies, explore how balances among nanoscale interactions are exploited for self-assembly and nanomanufacturing
- See papers on ctools

Self-assembly

1. ***attractive*** vs. ***repulsive*** interactions.
2. ***reversible*** association.

The magnitudes of interactions are generally fixed for molecules but can be engineered by:

- **Creating supramolecular building blocks**
- **Tuning the environment**
- **Applying external forces**

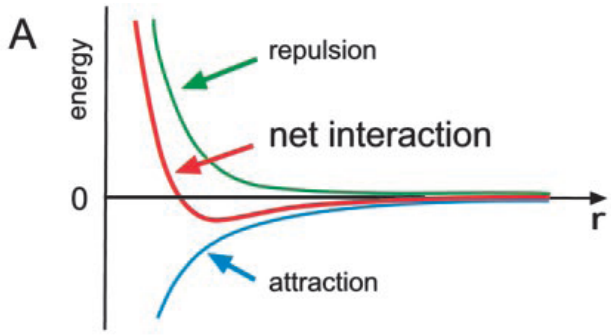

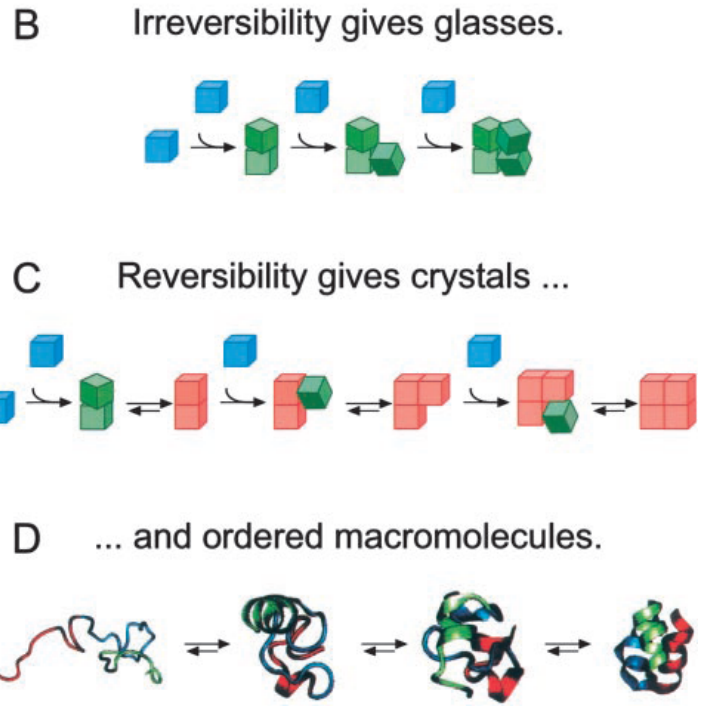

Whitesides and Boncheva, *PNAS 99(8):4769, 2002.*

Terms in the balance

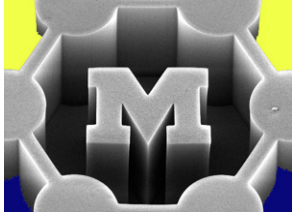

- Non-bonding interactions
  - "Locally" controlled
    - Intermolecular (VDW) forces
    - Elastic forces
    - Electrostatic forces
    - Steric hindrance (entropic)
  - "Remote control" means
    - Electric field
    - Magnetic field
    - Fluid flow
    - Ultrasonic agitation
    - Thermal field
- Bonding interactions

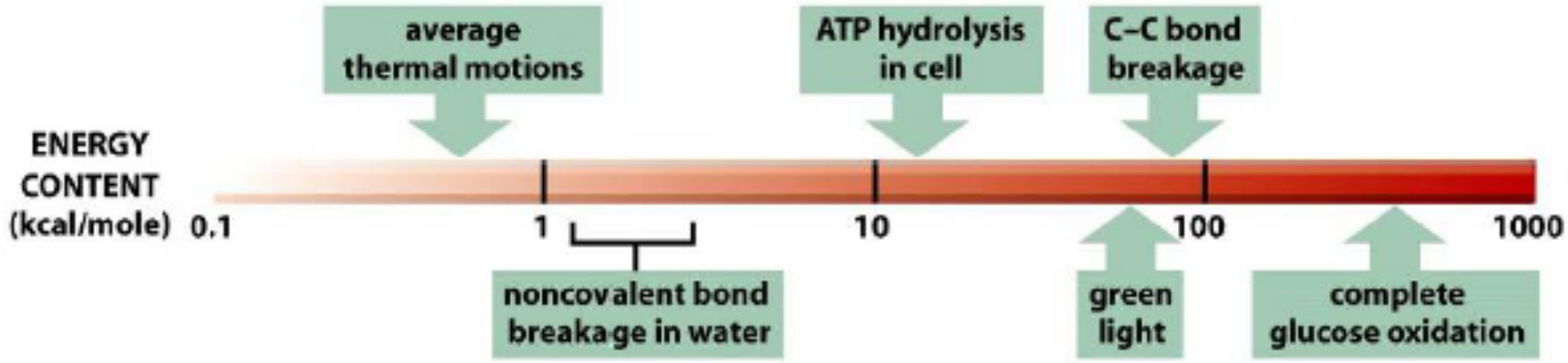

- Generally, weak non-covalent interactions are used in self-assembly

Alberts *et al.*, "Molecular Biology of the Cell," *5th edition.*

Sphere-templated nanoparticle rings

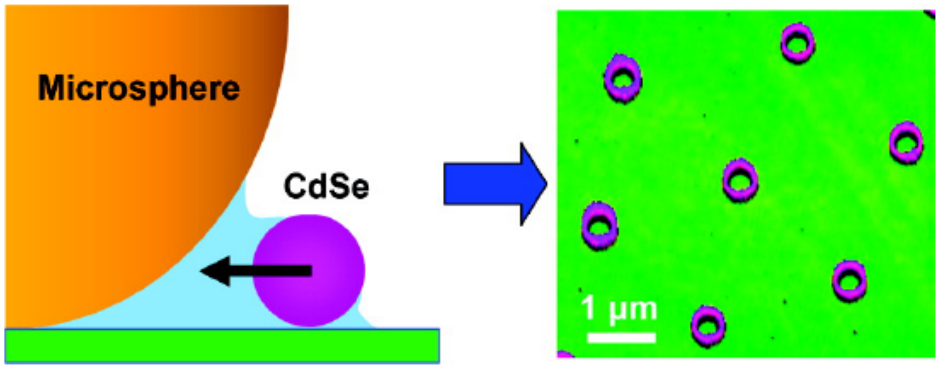

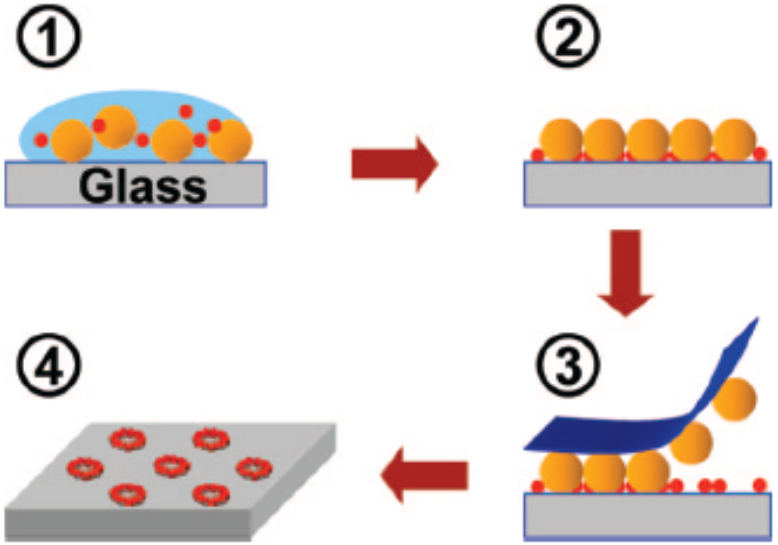

Figure 1. Schematic diagram of the evaporation templating procedure employed for forming CdSe nanorings (red particles) on planar substrates using microsphere templates (orange particles). Note that the drawing is not to scale.

- PS spheres: 10^{10}/mL
- QDs: 10^{14}/mL

Chen et al., *ACS Nano* 3(1):173-180, 2009.

Ring thickness control

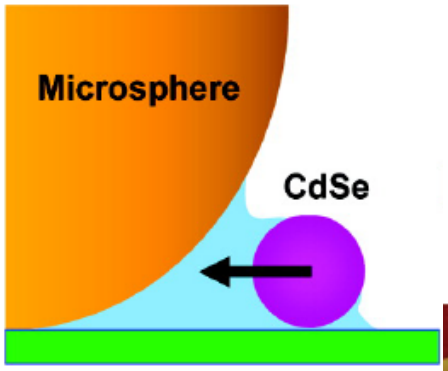

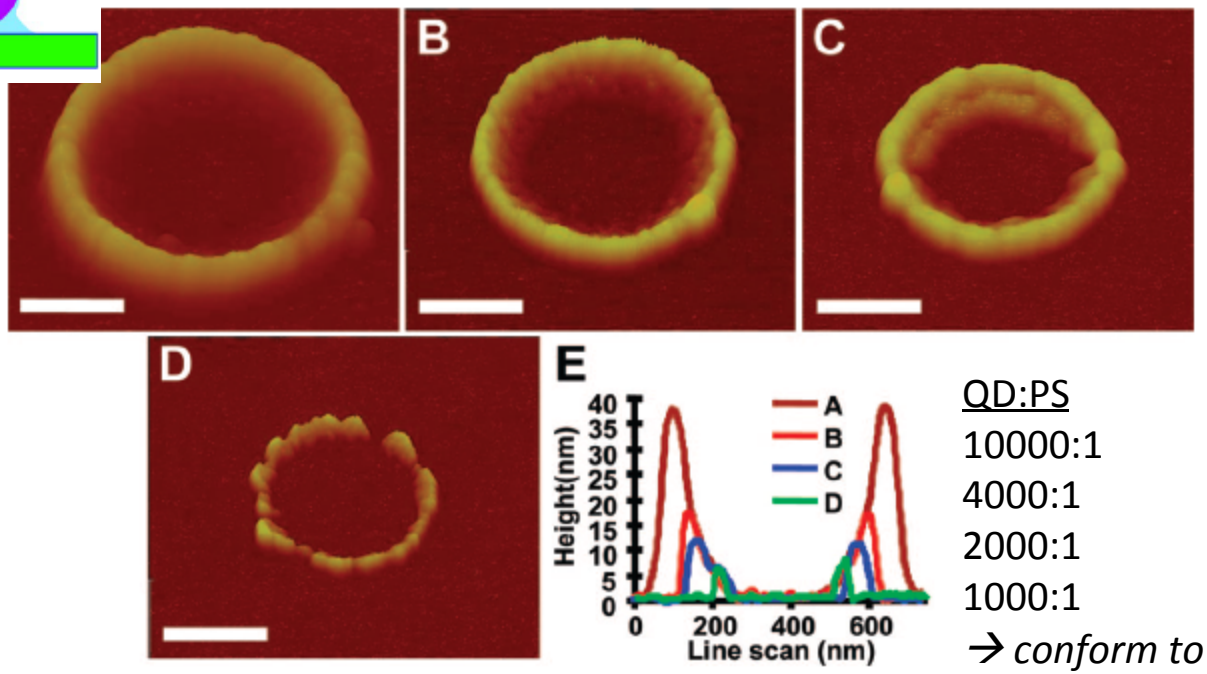

QD:PS
10000:1
4000:1
2000:1
1000:1
→ *conform to sphere*

Figure 5. AFM topographical 3D images of CdSe nanorings obtained from solutions using CdSe to polystyrene microsphere ratios of (A) 10000:1, (B) 4000:1, (C) 2000:1, (D) 1000:1. (E) Line profiles through the center of each ring. The scale bars in each image are 200 nm long.

Chen et al., *ACS Nano* 3(1):173-180, 2009.

Ring diameter control

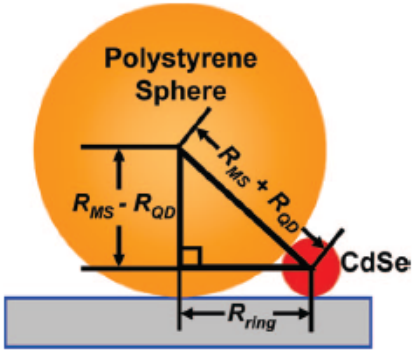

Figure 8. Schematic diagram of the hard sphere contact model employed for calculating the contact radius of the CdSe nanorings. Note that the drawing is not to scale.

$$R_{ring} = \sqrt{\left(R_{MS} + R_{QD}\right)^2 - \left(R_{MS} - R_{QD}\right)^2}$$

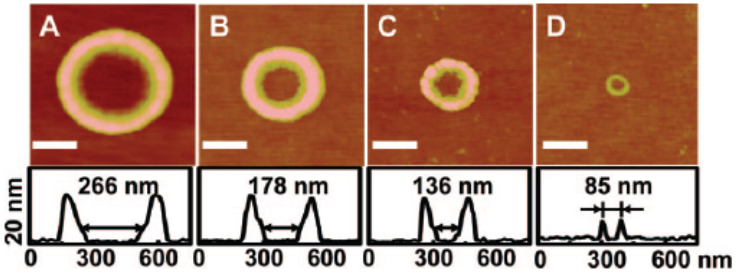

Figure 6. AFM topographical images and the corresponding line profiles from single CdSe nanorings formed with polystyrene spheres having diameters of (A) 2 μm, (B) 1 μm, (C) 600 nm, and (D) 200 nm. All scale bars are 200 nm long. The evaporative templating process was carried out at a CdSe concentration of 2×10^{13} QDs/mL under all conditions. The microsphere concentrations in the initial aqueous solutions were (A) 1×10^{10} spheres/mL, (B) 2×10^{10} spheres/mL, (C) 8×10^{10} spheres/mL, and (D) 3×10^{11} spheres/mL, respectively.

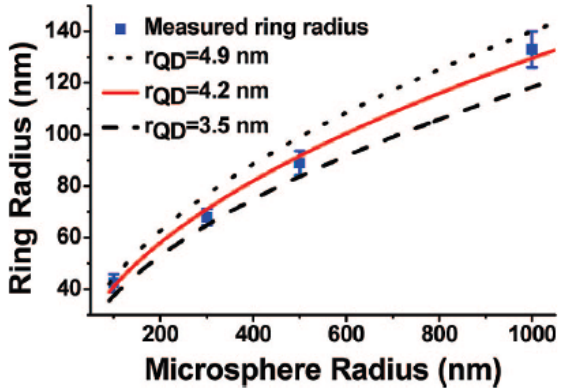

Figure 9. Plot of the CdSe ring radius *versus* the radius of the polystyrene sphere templates. The error bars on the data points are standard deviations from measurements of 20 separate nanorings. Curves were calculated using eq 1.

Chen et al., *ACS Nano* 3(1):173-180, 2009.

Self-assembled nanoparticle rings

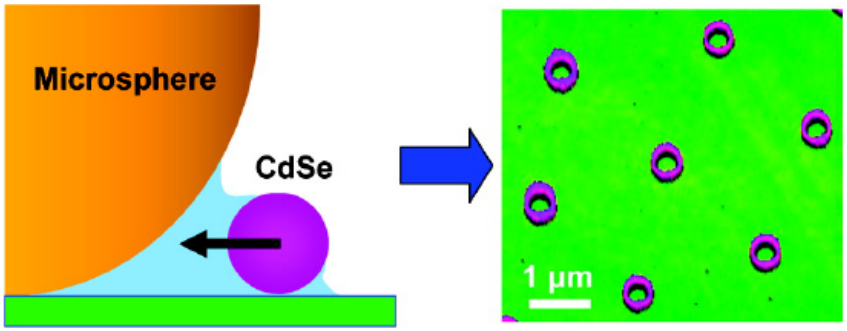

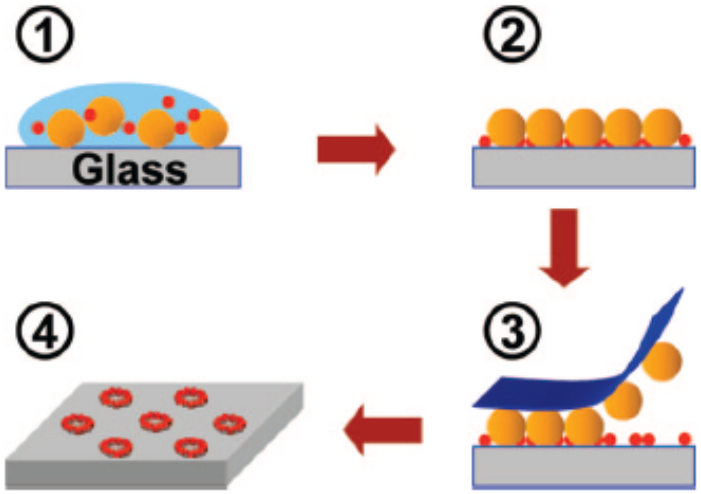

Figure 1. Schematic diagram of the evaporation templating procedure employed for forming CdSe nanorings (red particles) on planar substrates using microsphere templates (orange particles). Note that the drawing is not to scale.

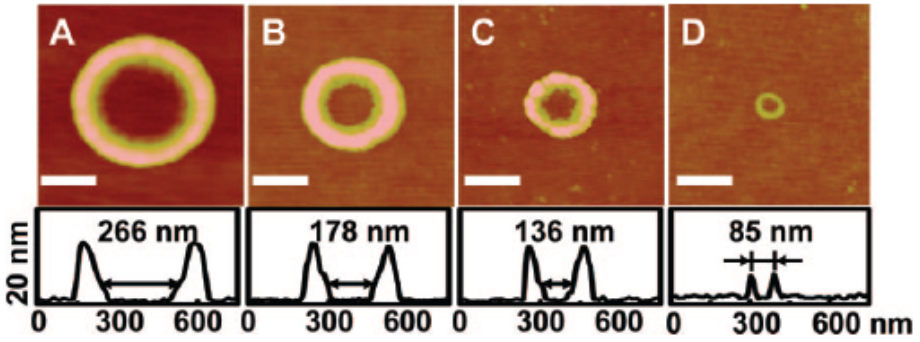

Figure 6. AFM topographical images and the corresponding line profiles from single CdSe nanorings formed with polystyrene spheres having diameters of (A) 2 μm, (B) 1 μm, (C) 600 nm, and (D) 200 nm. All scale bars are 200 nm long. The evaporative templating process was carried out at a CdSe concentration of 2×10^{13} QDs/mL under all conditions. The microsphere concentrations in the initial aqueous solutions were (A) 1×10^{10} spheres/mL, (B) 2×10^{10} spheres/mL, (C) 8×10^{10} spheres/mL, and (D) 3×10^{11} spheres/mL, respectively.

Chen et al., *ACS Nano* 3(1):173-180, 2009.

Force balance

- Capillary forces (attraction)
  - calculated $F_{cap} \leq 1.6$ nN ($r = 4$ nm)
  - total interaction energy ~400 kT

$$F_{cap} = 2\pi r\gamma\cos\theta$$

- Adhesion forces (attraction)
  - van der waals sphere-plane
  - calculated F_{ad} ~0.3 nN ($r = 4$ nm)

$$F_{ad} = \frac{A}{6z_0^2}\left(R + \frac{a^2}{z_0^2}\right)$$

- Electrostatic forces (repulsion)
  - point charge-plane; P is related to surface potential (difficult to predict)
  - calculated $F_{dl} < 1$ nN

$$F_{dl} = 2\pi R^2 Pe^{-kd}$$

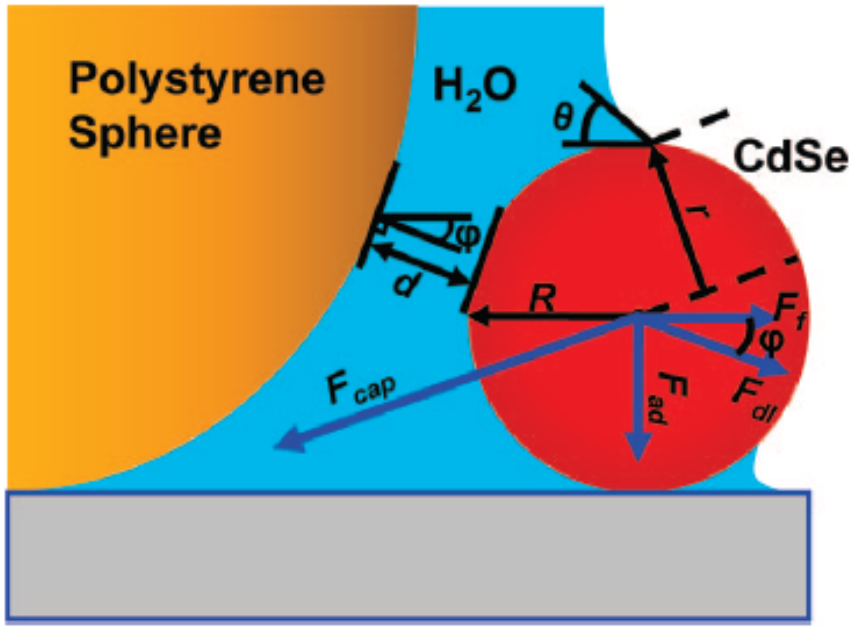

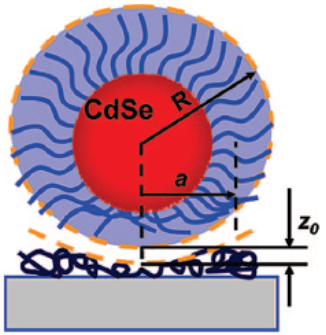

Figure 11. Schematic diagram of a 16-MHA capped CdSe quantum dot in contact with a PVP-modified glass substrate. Note that the drawing is not to scale.

Chen et al., *ACS Nano* 3(1):173-180, 2009.

Force balance

- Vector force addition predicts $F_{cap} > F_{dl} + F_{ad}$
- Also some friction (F_f)

- Note scaling

$$F_{cap} = 2\pi r\gamma \cos\theta$$

$$F_{dl} = 2\pi R^2 Pe^{-kd}$$

→ what happens as particle size increases?

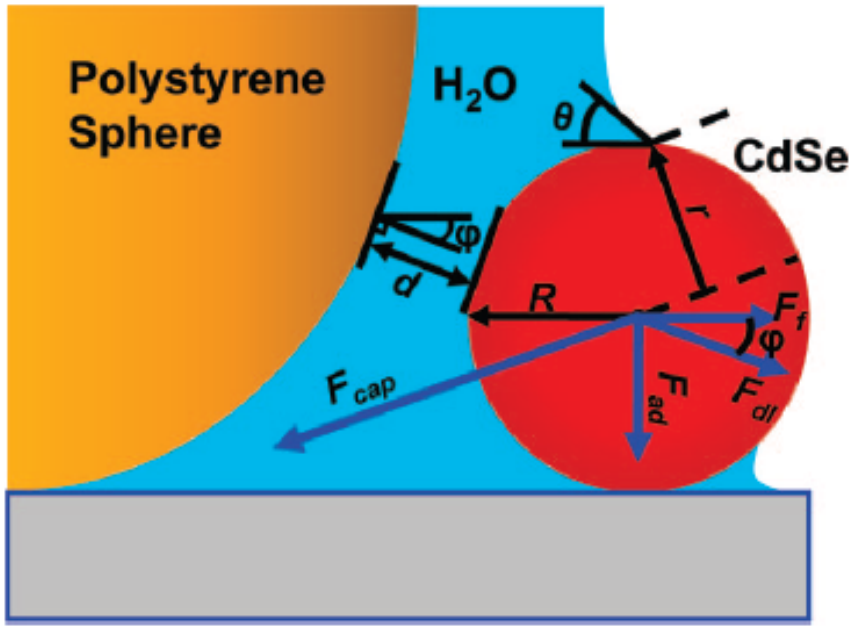

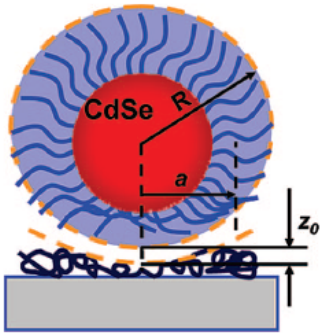

Figure 11. Schematic diagram of a 16-MHA capped CdSe quantum dot in contact with a PVP-modified glass substrate. Note that the drawing is not to scale.

Chen et al., *ACS Nano* 3(1):173-180, 2009.

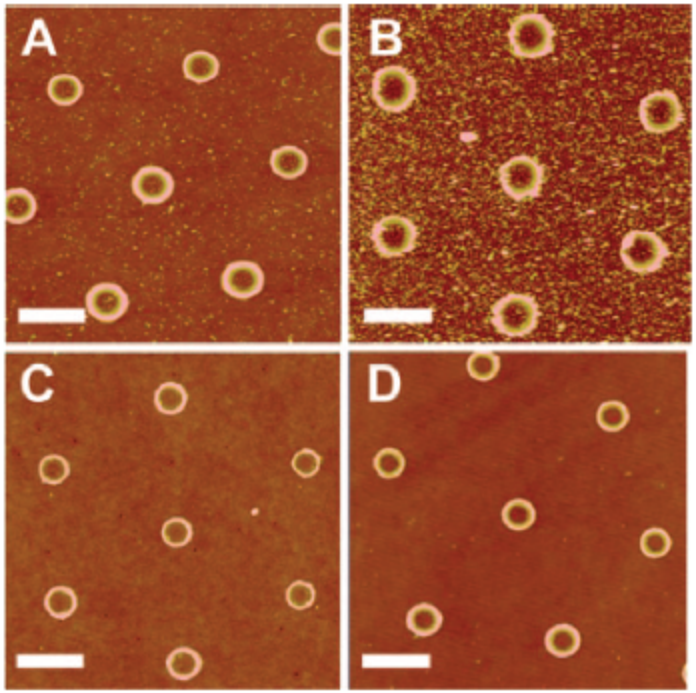

(A: clean, B: acid-modified) Too many QDs stick to substrate

(C) Not enough adhesion (QDs wash off in water)

(D) Just right (intermediate adhesion, stable when washed)

Figure 2. AFM topographical images of CdSe rings on (A) clean glass, (B) APTMS-modified glass, (C) Shipley 1805 photoresist coated glass, and (D) PVP-modified glass. The scale bars are each 1 μm long.

Chen et al., *ACS Nano* 3(1):173-180, 2009.

Templated particle assembly

Geometric shape of the template	Structure of the cluster	Requirements
D	d	D/d = 1.00-2.00
		D/d = 2.00-2.15
		D/d = 2.15-2.41
		D/d = 2.41-2.70
		D/d = 2.70-3.00
		D/d = 3.00-3.30
a		a = 2d
L W		L = 4d W = d
		d < w < 2d
L		L = 2.73d
D D'		D = 3d D' = d

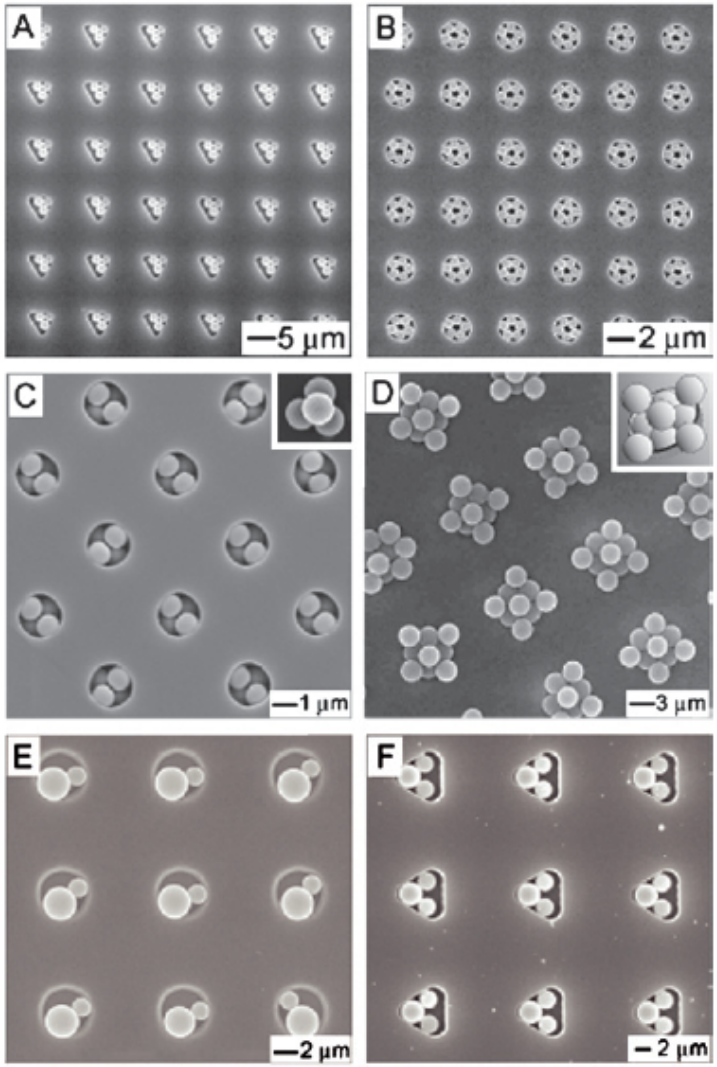

Rycenga et al., *Soft Matter* 5:1129-1136, 2009.

Templated assembly assisted by ultrasonic agitation

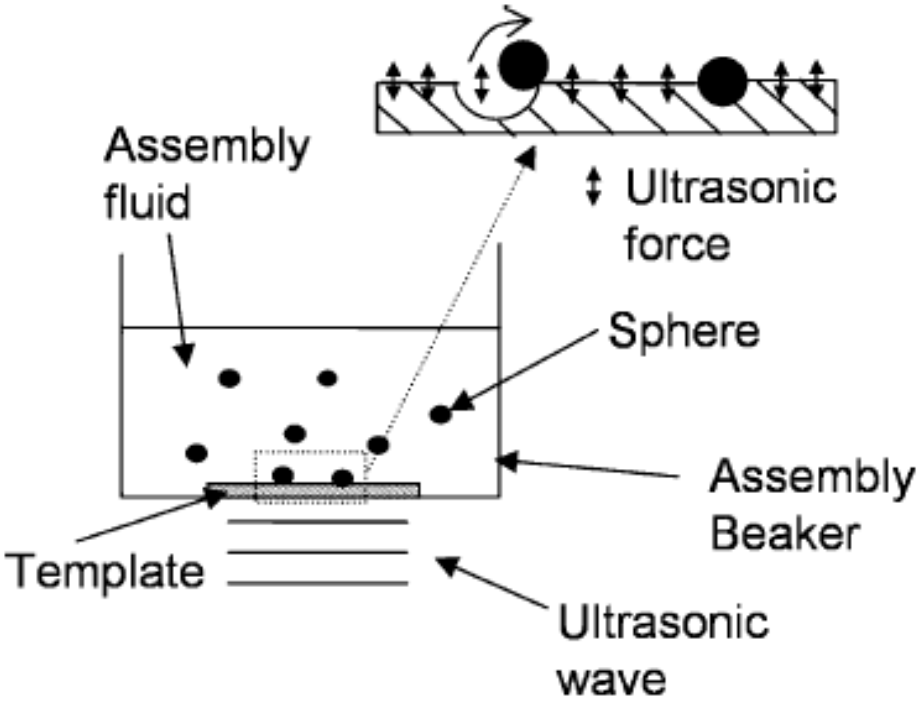

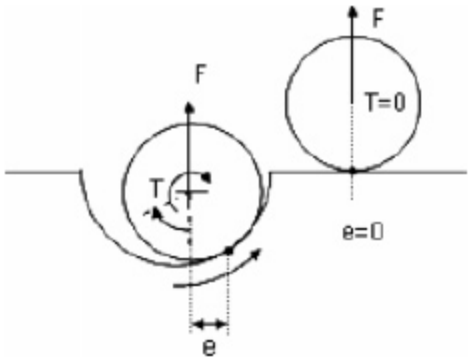

Figure 6. Cross-sectional schematic of a sphere in a hole and a sphere on a flat surface, along with forces and torques acting on the spheres. Vertical forces acting at the center of the sphere in the hole create a torque around the contact point that tends to roll the sphere up the sidewall. Vertical forces acting at the center of the sphere on the flat surface create no torque.

Jung and Livermore, *Nano Letters* 5(11):2188-2194

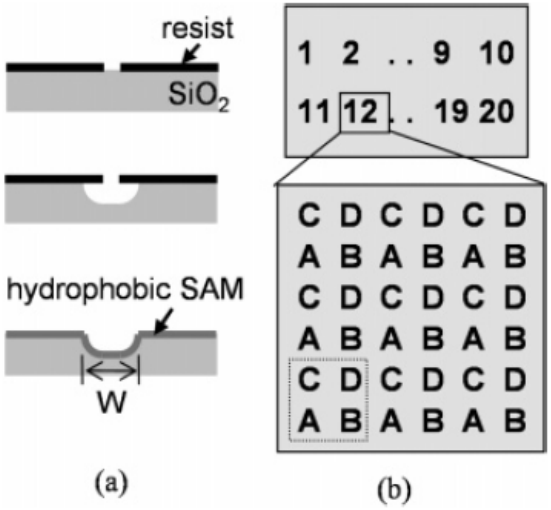

Figure 2. (a) Substrate fabrication process: coat oxidized silicon wafer with PMMA and pattern small hole with e-beam lithography; etch oxide to form a near-hemispherical hole; and coat surface with hydrophobic SAM. (b) Pattern layout includes 20 arrays, identical but with increasing exposure dose to form increasingly large holes; close-up of an array showing repeated pattern of four hole shapes (A, B, C, D) corresponding to four different-sized exposure regions.

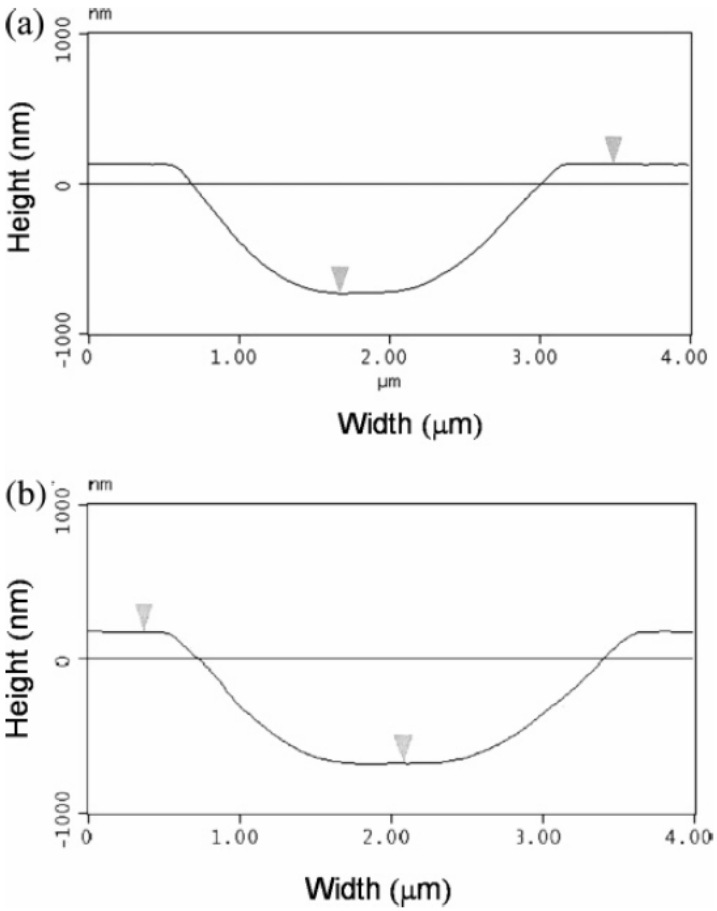

type A

type D

Figure 5. Profile of (a) a sample type A hole and (b) a sample type D hole, measured by AFM.

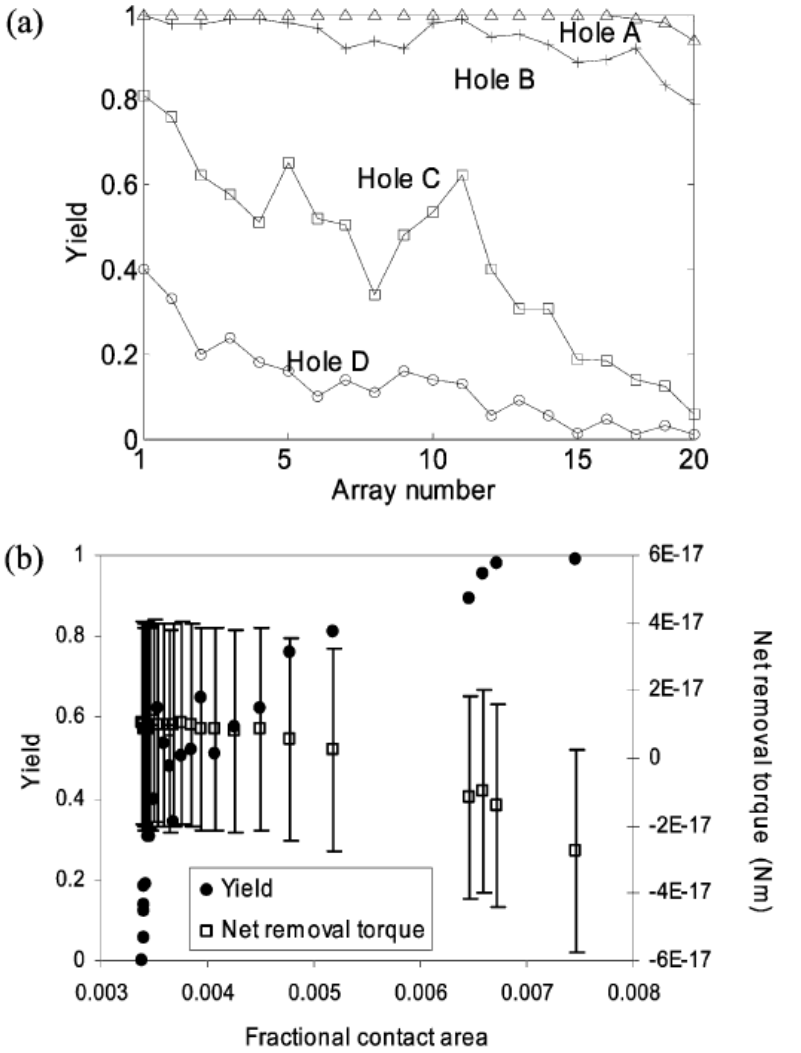

Figure 4. (a) Yield vs exposure number for type A, B, C, and D holes. Higher array number indicates higher exposure dose. (b) Yield vs nominal fractional contact area (left axis) and net removal torque vs nominal fractional contact area (right axis).

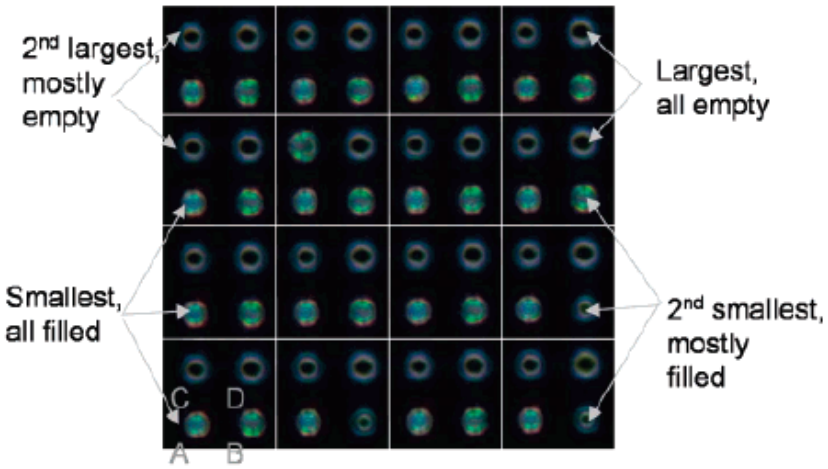

Figure 3. Optical micrograph of assembly results for the array with largest exposure dose. Filled holes appear solid, and empty holes appear hollow. Grid lines are guides to the eye and identify groups of type A, B, C, and D holes.

Isolated CNTs: bridging

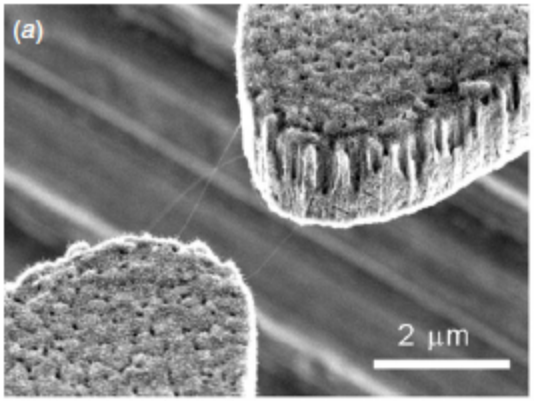

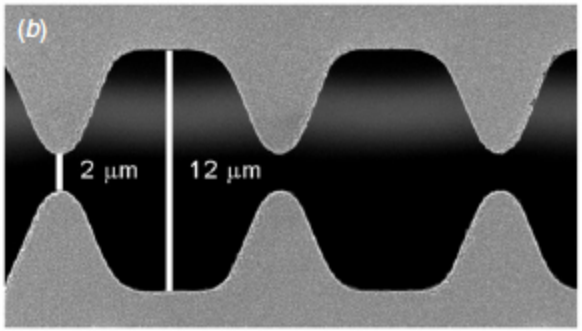

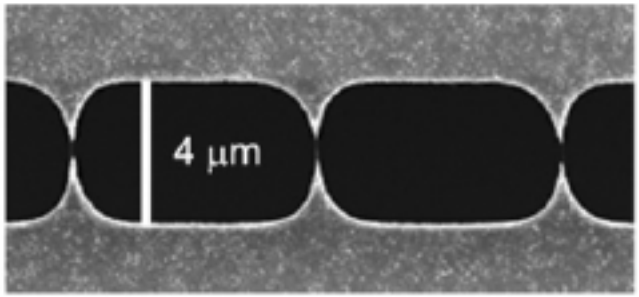

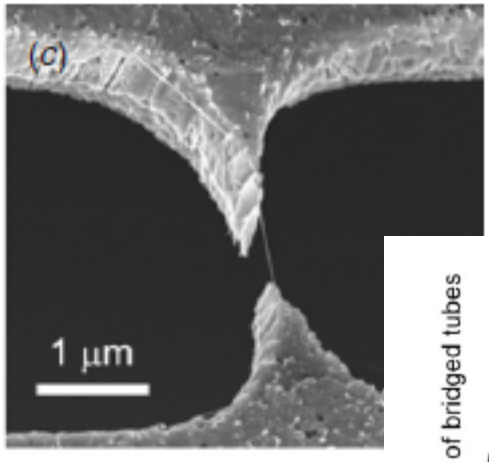

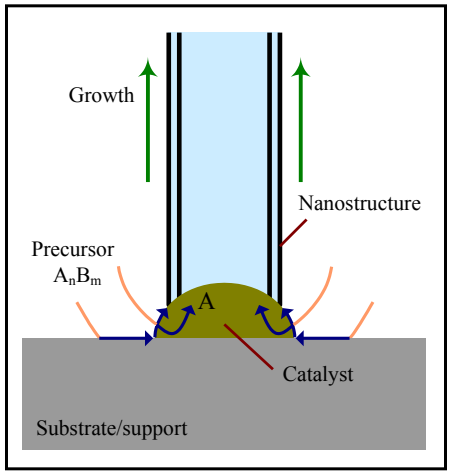

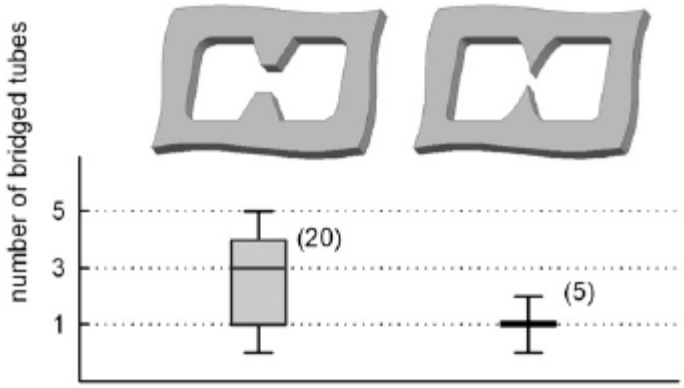

Figure 6. Box plot of two different tip apex geometries. Figures in parenthesis indicate the number of measured tip pairs. The ultra-sharp tips have a mean number of spanned SWNT of 1 tube per tip pair.

Jungen et al., *J. Micromech Microeng.*, 17:603-608, 2007.

Electric field-directed CNT growth

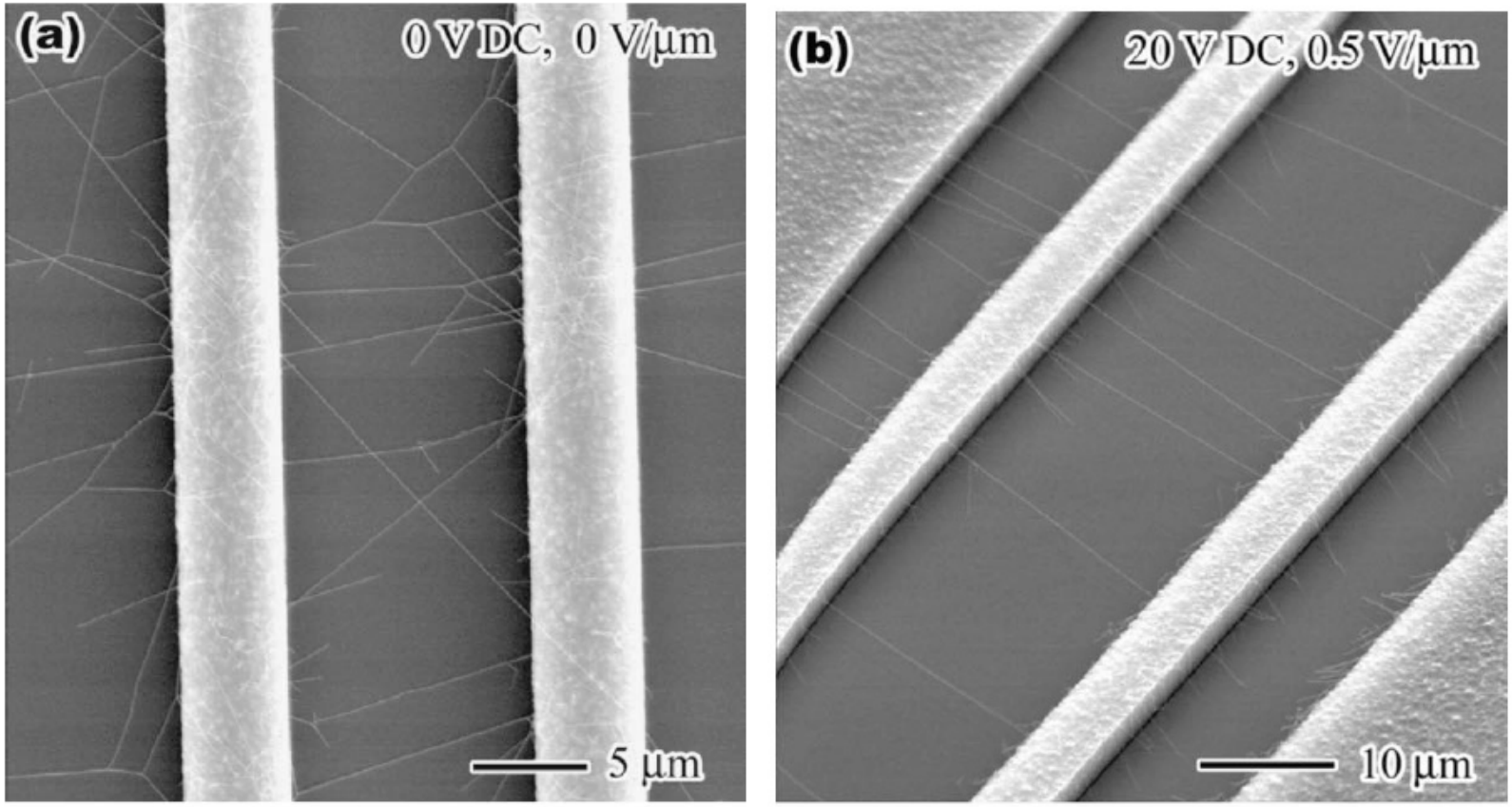

Zhang et al., *Applied Physics Letters* 79(19):3155:3157, 2001

Electric field-directed CNT growth

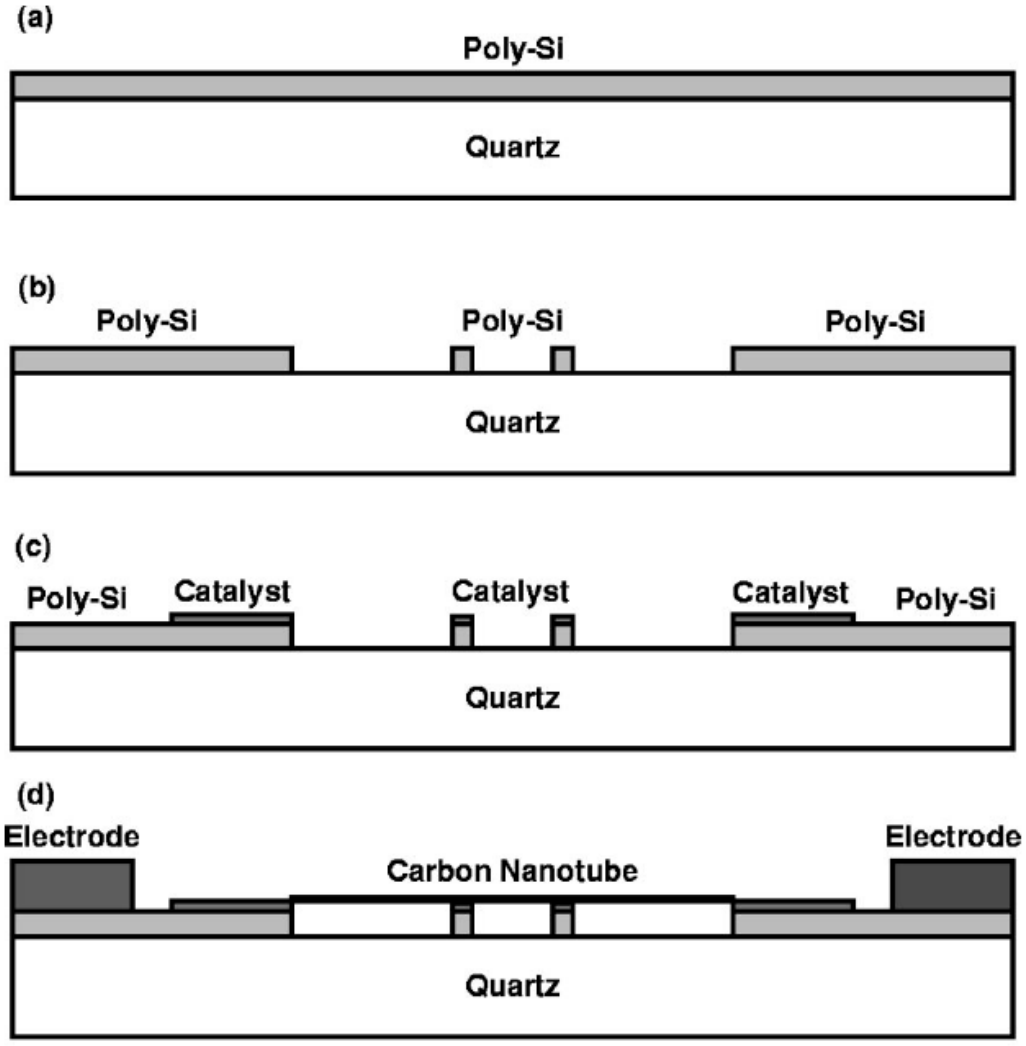

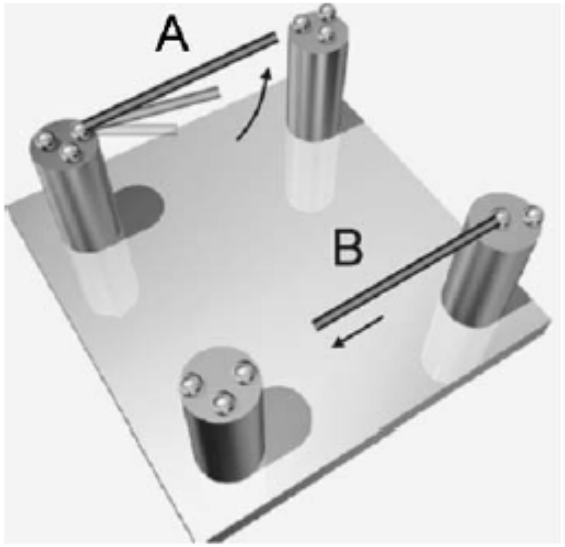

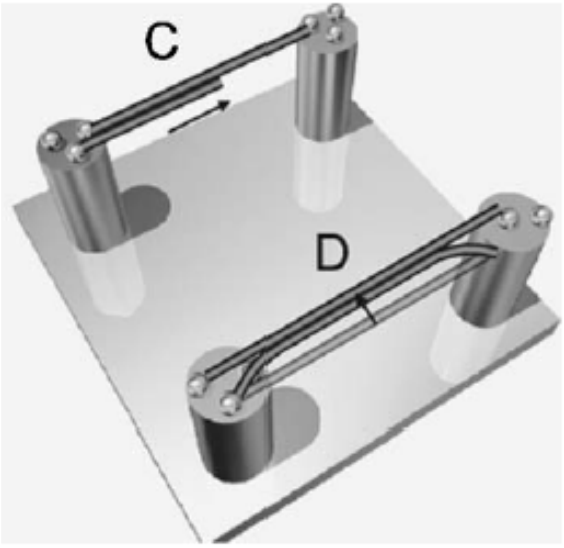

Zhang et al., *Applied Physics Letters* 79(19):3155:3157, 2001
Homma et al., *Applied Phys Letters* 88, 2006

For a CNT at 900 °C with d = 2 nm, L = 20 µm

- With no applied field, tip vibration = 6.3 µm!
- With 1 V/µm, tip vibration = 0.6 µm

$$F_R = \alpha_{||} E^2 \sin\theta\cos\theta / L$$

Alignment force

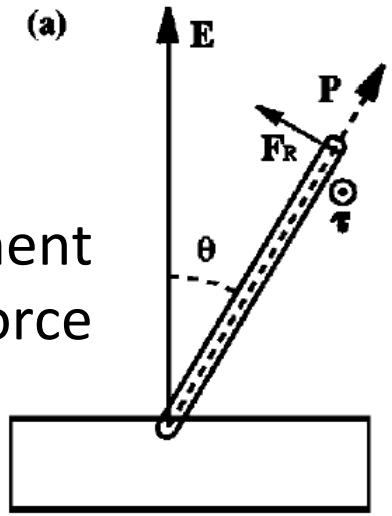

$$\delta = \left\{ \frac{0.846 L^3 kT}{YdG\left(d^2 + G^2\right)} \right\}^{1/2}$$

Thermal vibration

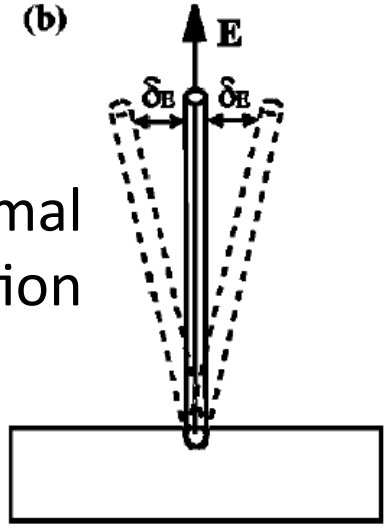

- Higher field needed to align longer CNTs

Zhang et al., *Applied Physics Letters* 79(19):3155:3157, 2001
Homma et al., *Applied Phys Letters* 88, 2006

No field alignment when CNTs are not suspended

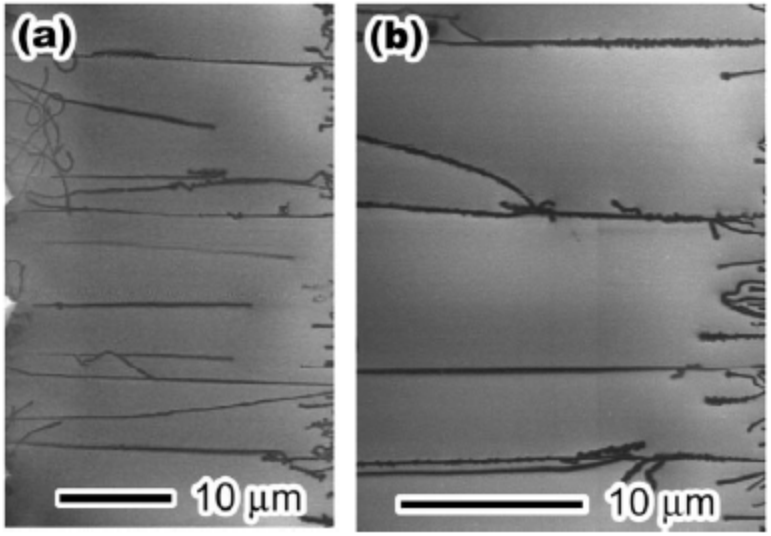

FIG. 5. SEM images of SWNTs (dark lines) at the bottom of the trenches grown under an applied dc voltage of 50 μm. The spacing between the outer poly-Si electrodes is 100 μm.

- See methods of lateral CNT growth on single-crystal substrates (e.g., quartz or miscut sapphire)

Zhang et al., *Applied Physics Letters* 79(19):3155:3157, 2001

Electrophoresis: placing particles in gaps

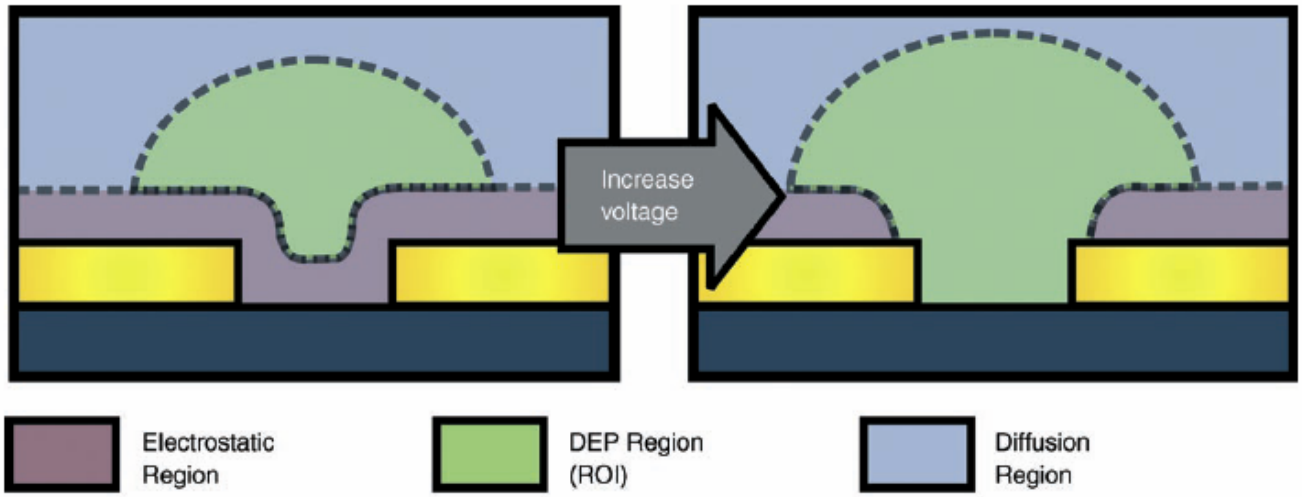

Figure 7. Schematic image showing regions where different forces dominate during DEP assembly of nanoparticles into nanogaps at voltages lower (left) and higher (right) than the threshold voltage.

- Motion is diffusive (Brownian) far from gap
- Substrate-particle repulsion dominates at low V
- "Spherical" DEP region grows and dominates at high V
- EP-induced oscillation only important at low frequencies

Barsotti et al., Small 3(3):488, 2007.

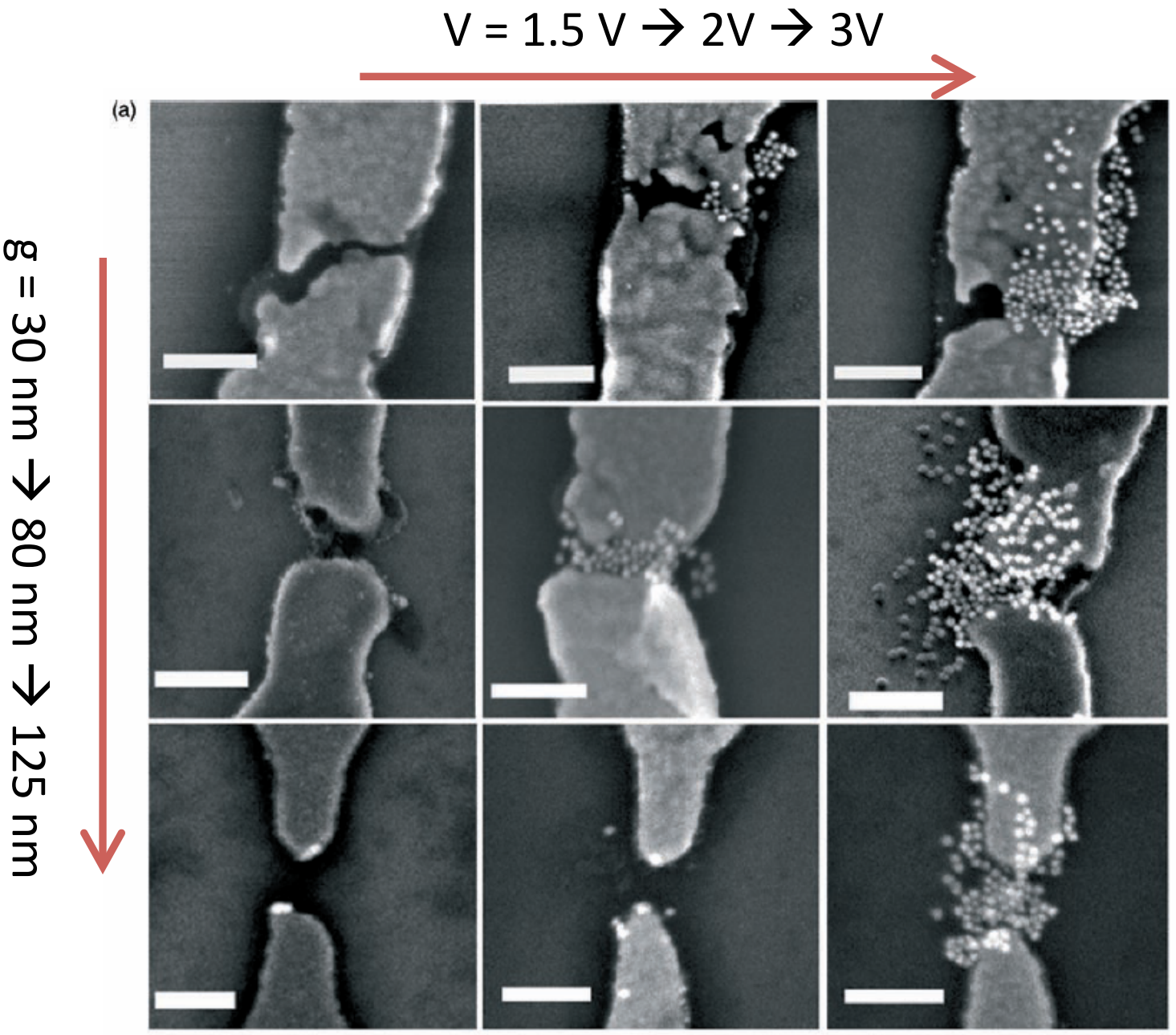

Barsotti et al., *Small* 3(3):488, 2007.

Silicon nanopillar arrays

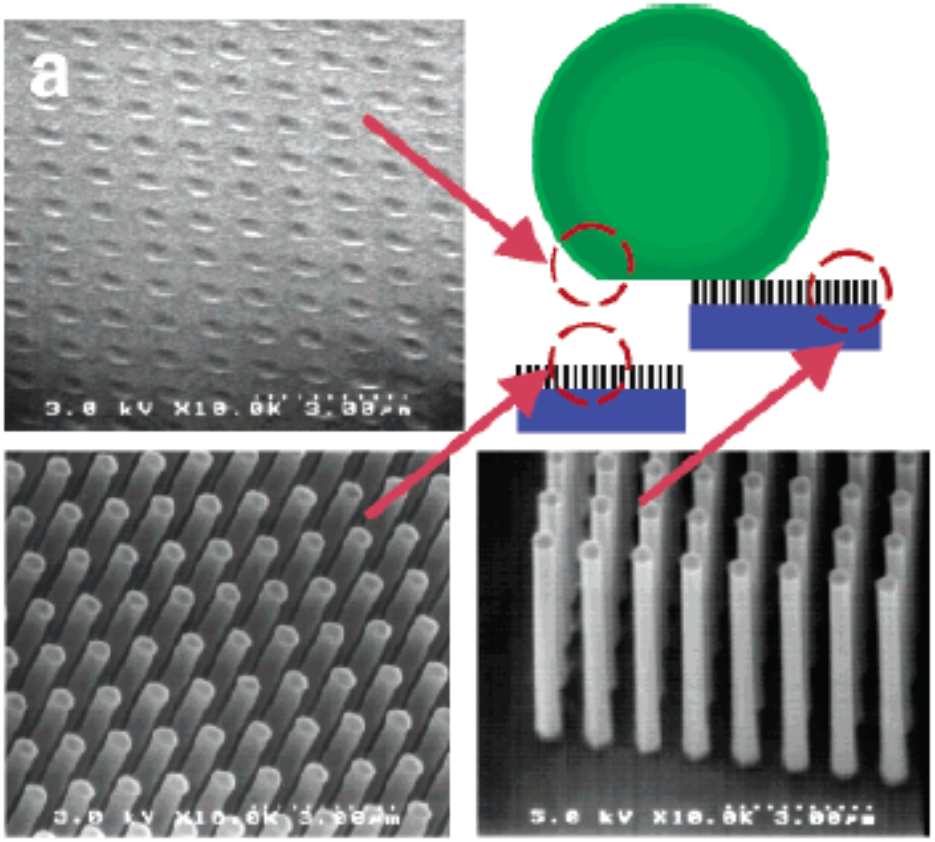

Krupenkin et al., *Langmuir* 20:3824-3827, 2004.

Making polymer nanopillars by replication

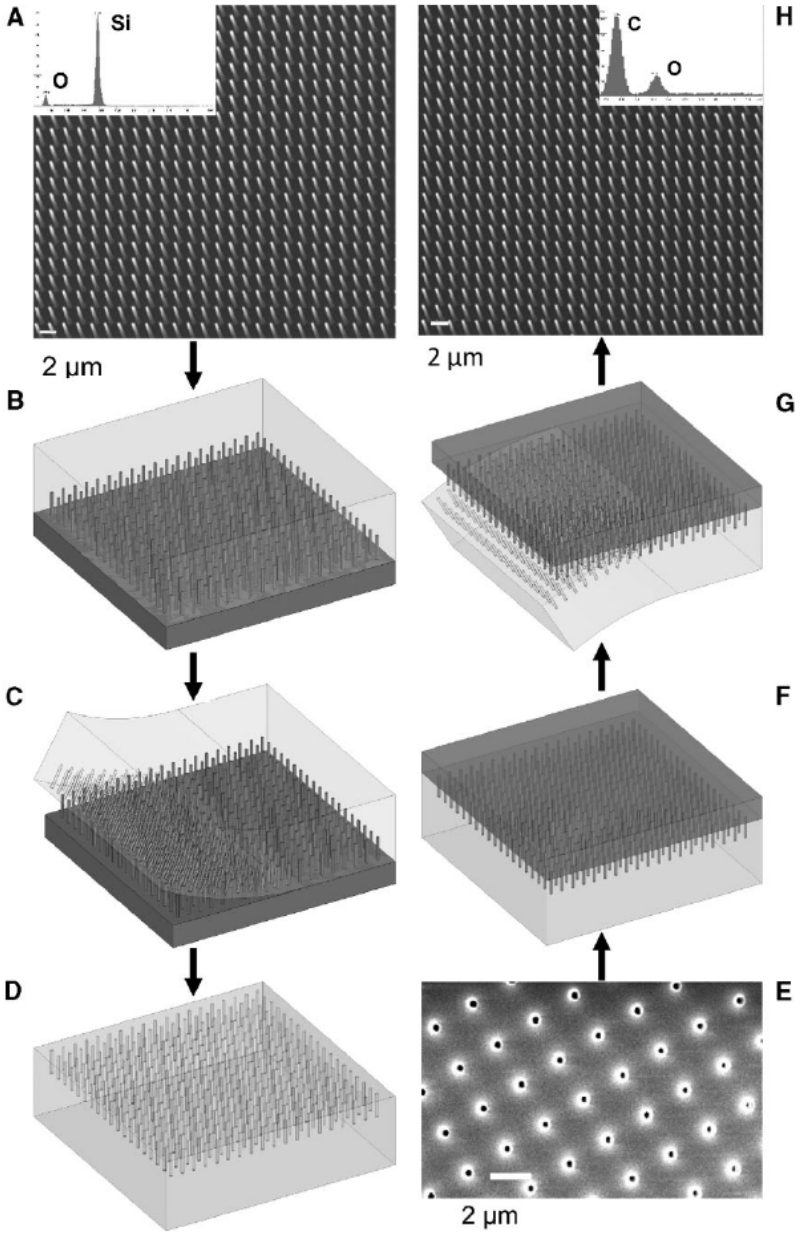

Figure 1. Two-step soft-lithography process for creating replicas of nanostructured surfaces with high-aspect-ratio features. A) SEM image of an exemplary original nanostructured surface—a silicon master bearing a square array of posts 8 µm long with the diameter 250 nm and pitch 2 µm. The oblique view is used to best visualize the structure. The insert is an EDS spectrum. B) Liquid PDMS precursor is poured onto the master, treated with an antisticking agent, and cured. C) The cured PDMS is peeled off from the master. D) The negative PDMS mold, which contains an array of high-aspect-ratio wells corresponding to the posts of the positive master, is surface-treated with an antisticking agent. E) SEM image of the PDMS mold, revealing the high-aspect-ratio wells. F) Liquid precursor (polymer, liquid metal) is poured onto the negative PDMS mold and cured. G) The PDMS mold is peeled from the cured positive replica. H) SEM image of an exemplary nanostructured replica fabricated from epoxy resin. The insert is an EDS spectrum. The replicated structure is geometrically indistinguishable from the master shown in A).

Pokroy et al., Advanced Materials 21:463-469, 2009.

Elastocapillary coalescence

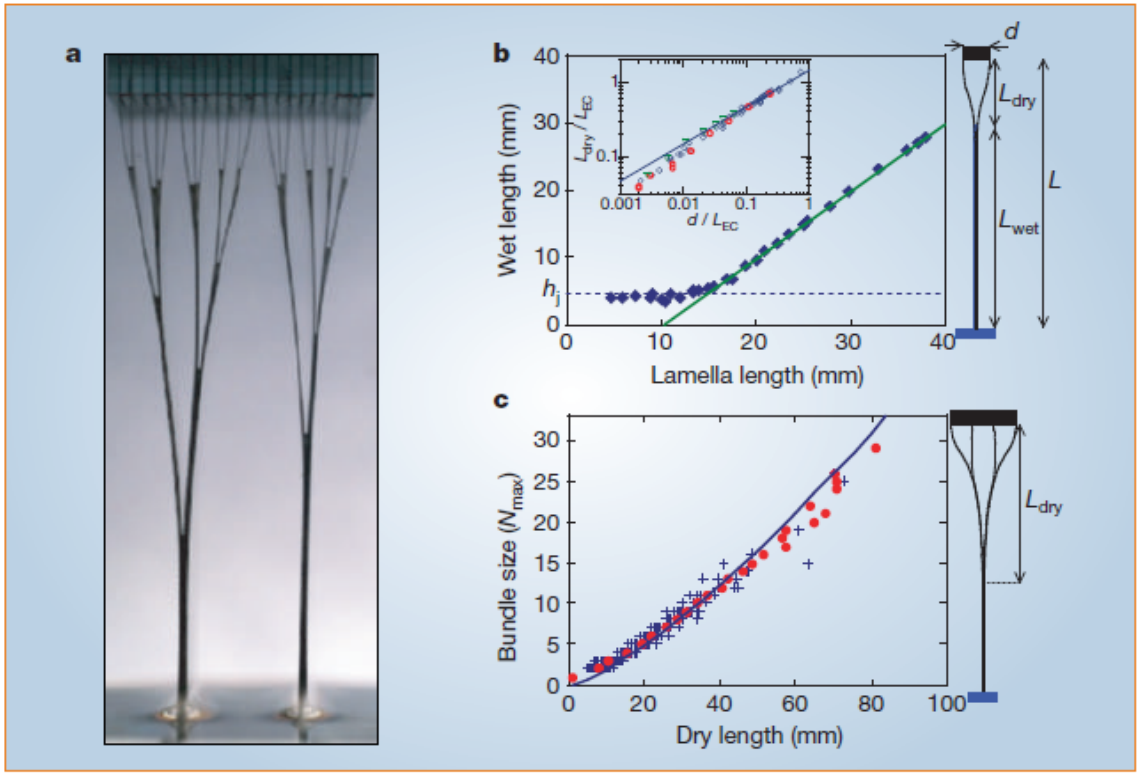

Figure 1 Flexible lamellae stick together after wetting. **a,** Lamellae in a wetted model brush after a sequence of sticking or unsticking events that cause aggregation (viewing from top to bottom) or fragmentation (from bottom to top), respectively. **b,** Height of rise, L_{wet}, of liquid between a lamella pair is plotted against the withdrawal height, L, showing the transition from the capillary rise (dashed line; $L_{wet}=h_j$) to the sticking regime (full green line; $L_{dry}=L-L_{wet}$ is constant). Polyester strips separated by $d=1$ mm (width, 25 mm; thickness, $e=100$ μm; bending rigidity, $\kappa=5.1\times10^{-4}$ N m) were dipped into silicon oil (density, $\rho=950$ kg m^{-3} and surface tension $\gamma=20.6$ mN m^{-1}, leading to $h_j=4.3$ mm). Inset, sticking regime. Non-dimensional dry length, L_{dry}/L_{EC}, is plotted against non-dimensional separation, d/L_{EC}; $L_{EC}=(\kappa/\gamma)^{1/2}$, which is the elastocapillary length (red circles: $e=50$ μm, $L_{EC}=47$ mm; blue diamonds: $e=100$ μm, $L_{EC}=150$ mm; green triangles: $e=170$ μm, $L_{EC}=370$ mm); line: comparison with theory (equation (1); no adjustable parameter). **c,** Aggregation of multiple lamellae into bundles ($e=50$ μm, $d=1$ mm). Number of lamellae per bundle is plotted against dry length. Blue crosses, raw data; red circles, averaging of data; line, comparison with theory (equation (2); no adjustable parameter).

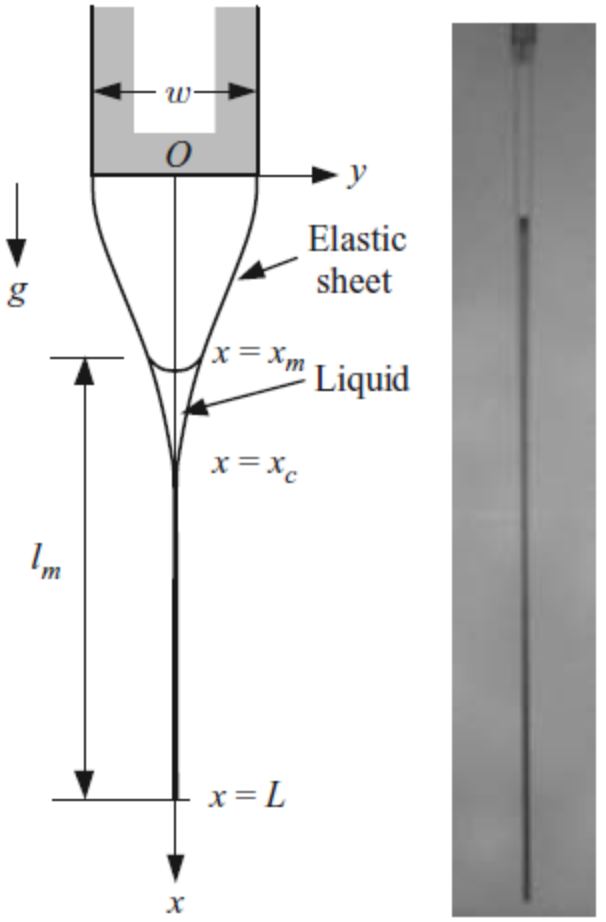

Bico et al., *Nature* 432:690, 2004.

Kim and Mahadevan, *J. Fluid Mech.* 548:141, 2006.

Hierarchical grouping of polymer nanopillars

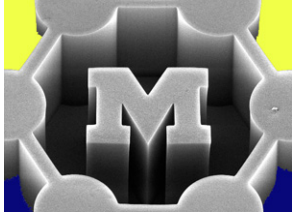

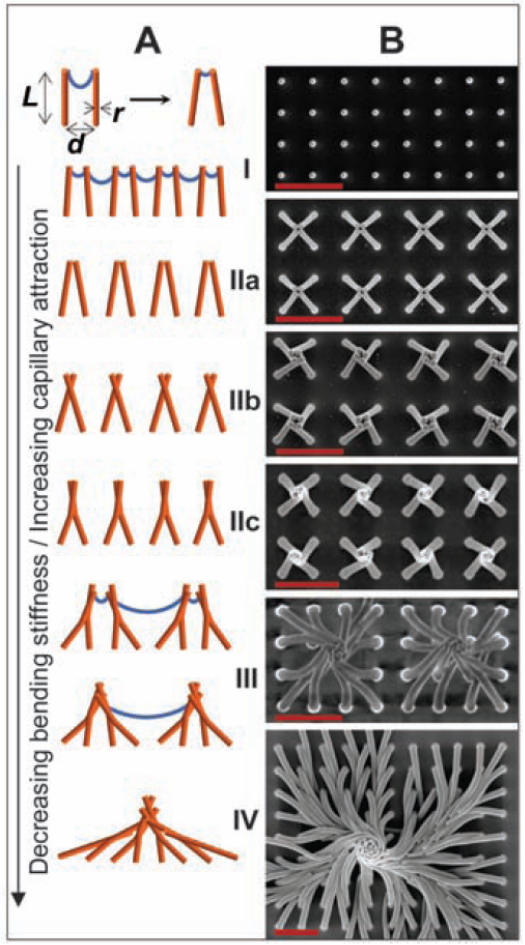

Fig. 1. (**A**) Schematic diagrams and (**B**) corresponding scanning electron microscopy (SEM) images showing the morphogenesis of helical patterns, from the first-order unclustered nanobristle to the fourth-order coiled bundle. Scale bars, 4 μm. Note the hierarchical nature of the assembly reflected in the presence of the lower-order braids in the large clusters braided in a unique structure reminiscent of modern dreadlocks or mythical Medusa.

- Bending energy (force)
- Capillary force
- Adhesion energy (force)

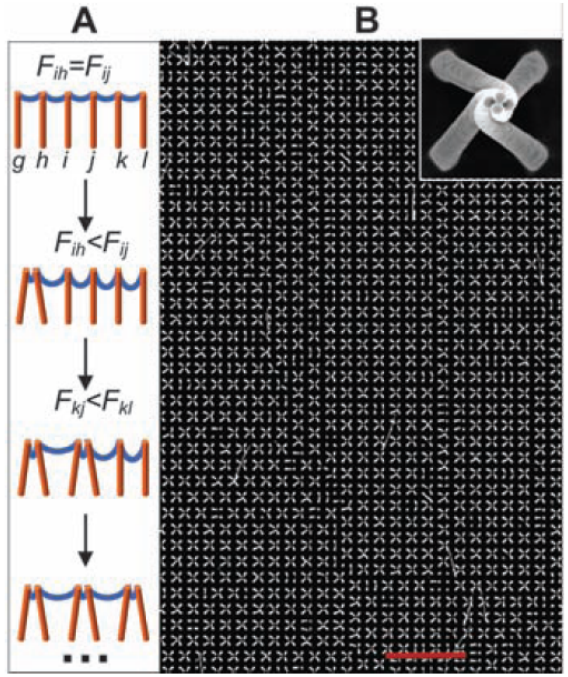

Fig. 2. Large-area self-organization of the bristle. (**A**) Schematic diagram showing the mechanism of the formation of the long-range order in the assembled bristle. See text for further details. (**B**) SEM image showing the assembly into uniform, periodic fourfold clusters of nanopillars over the submillimeter area. Note the different coherent domains that arise from the multiple nucleation sites. Scale bar, 20 μm.

Pokroy et al., *Science* 323:237-240, 2009.

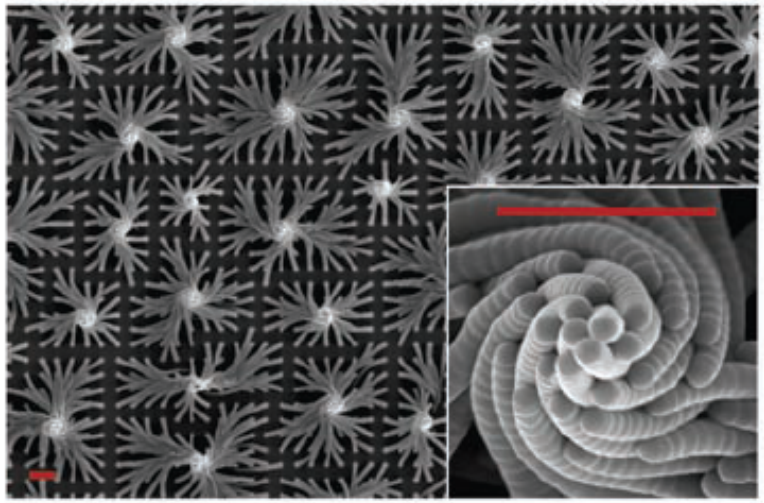

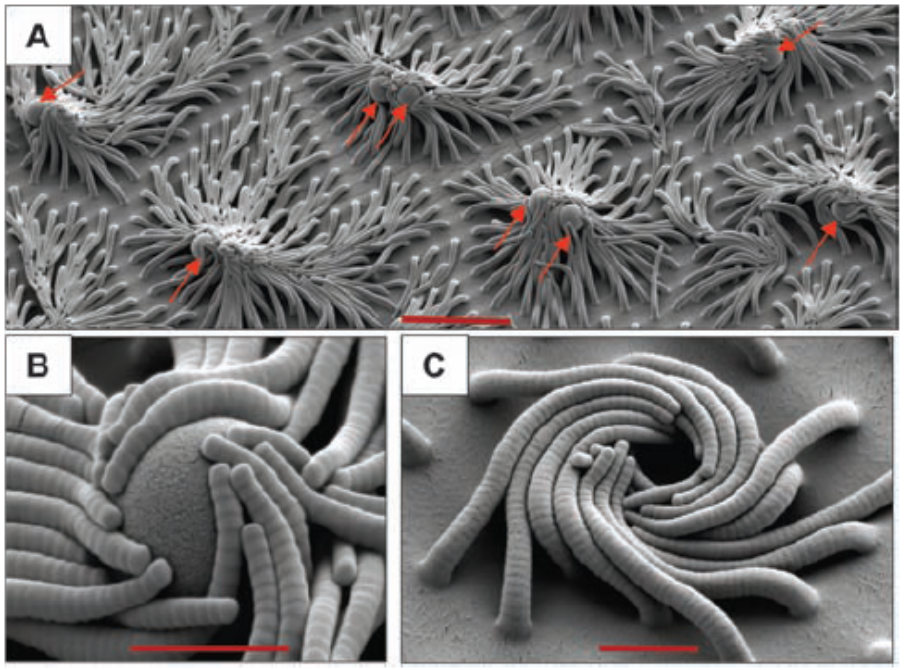

Fig. 5. Illustration of the adhesive and particle-trapping potential of the helically assembling bristle. (**A**) Low-magnification SEM showing the capture of the 2.5-μm polystyrene spheres (indicated by arrows). Scale bar, 10 μm. (**B**) Magnified view depicting a single sphere trapped through the conformal wrapping of the nanobristle. Scale bar, 2 μm. (**C**) Coiled whirlpools remain after the removal of the spheres. Scale bar, 2 μm.

Pokroy et al., *Science* 323:237-240, 2009.

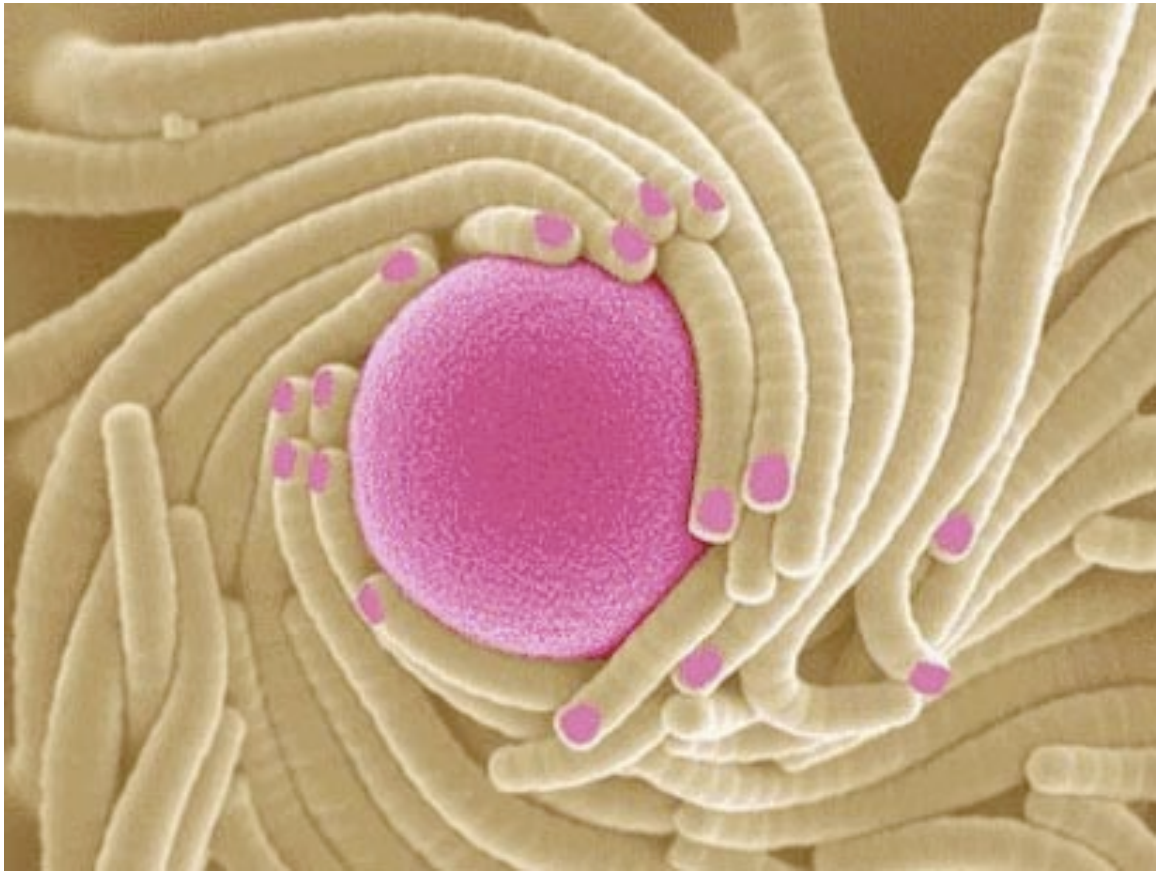

Aizenberg group, Harvard. First Place, *MRS Science as Art*, December 2008

Elastocapillary densification of CNT forests

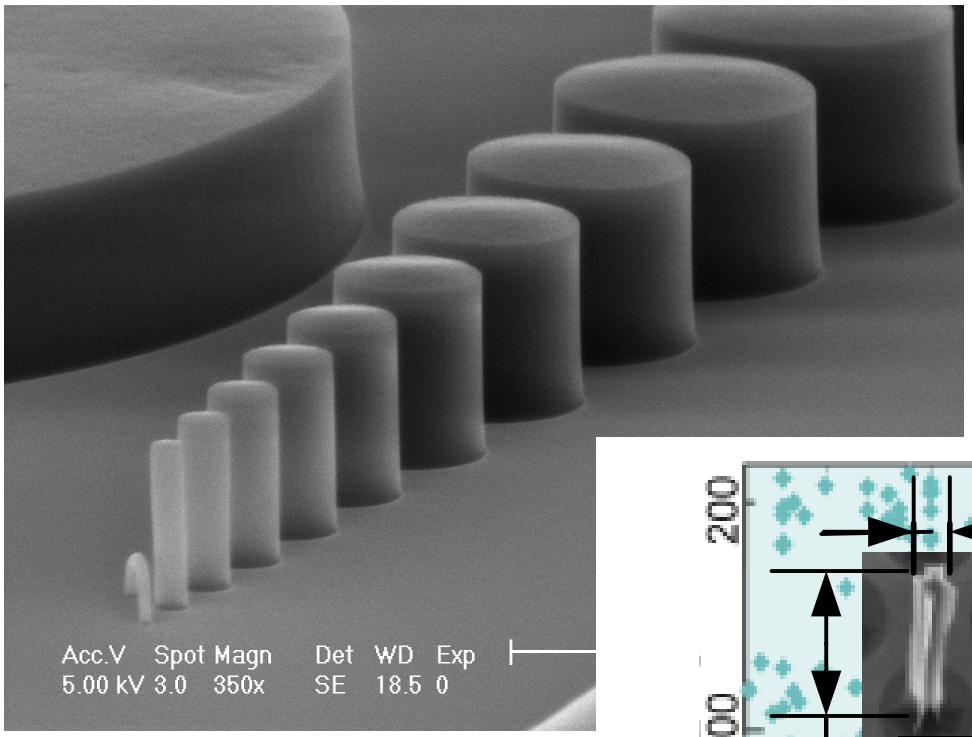

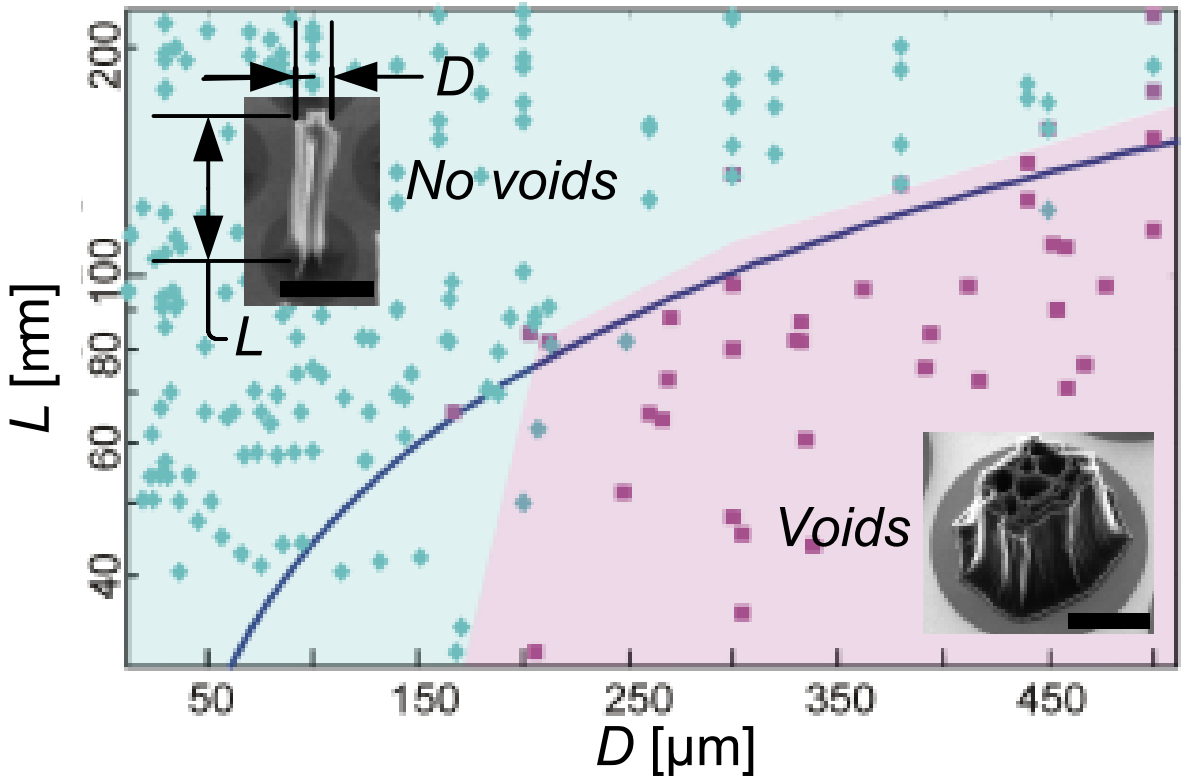

De Volder, Tawfick, Park, Hart.

Mechanical properties of densified CNTs

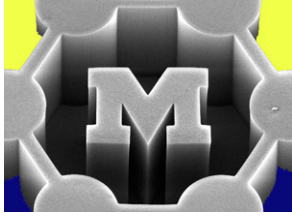

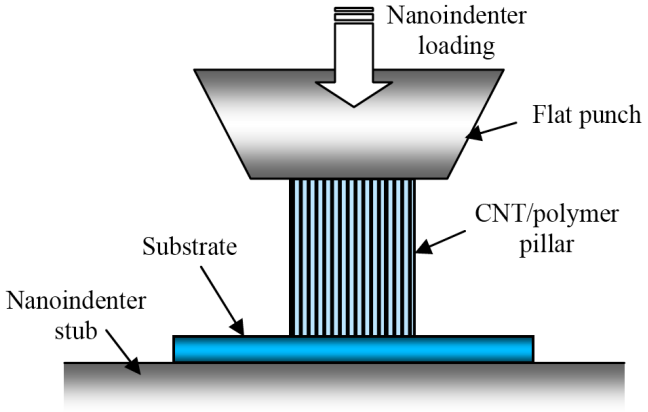

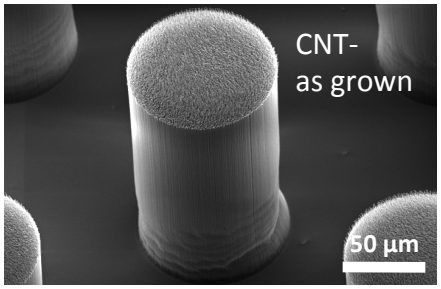

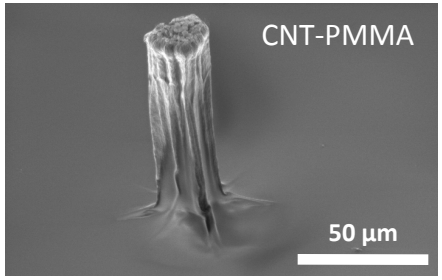

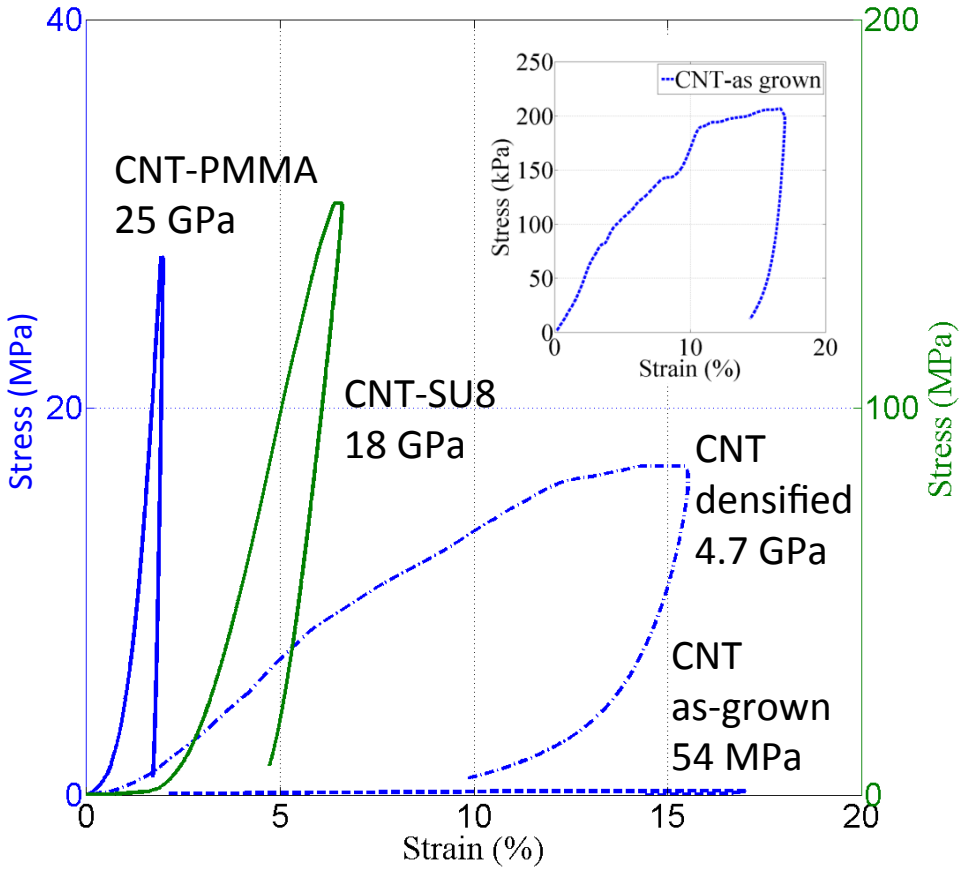

DNA (Deoxyribonucleic acid)

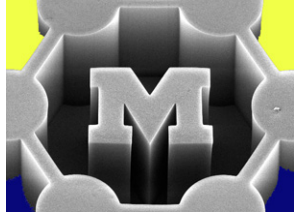

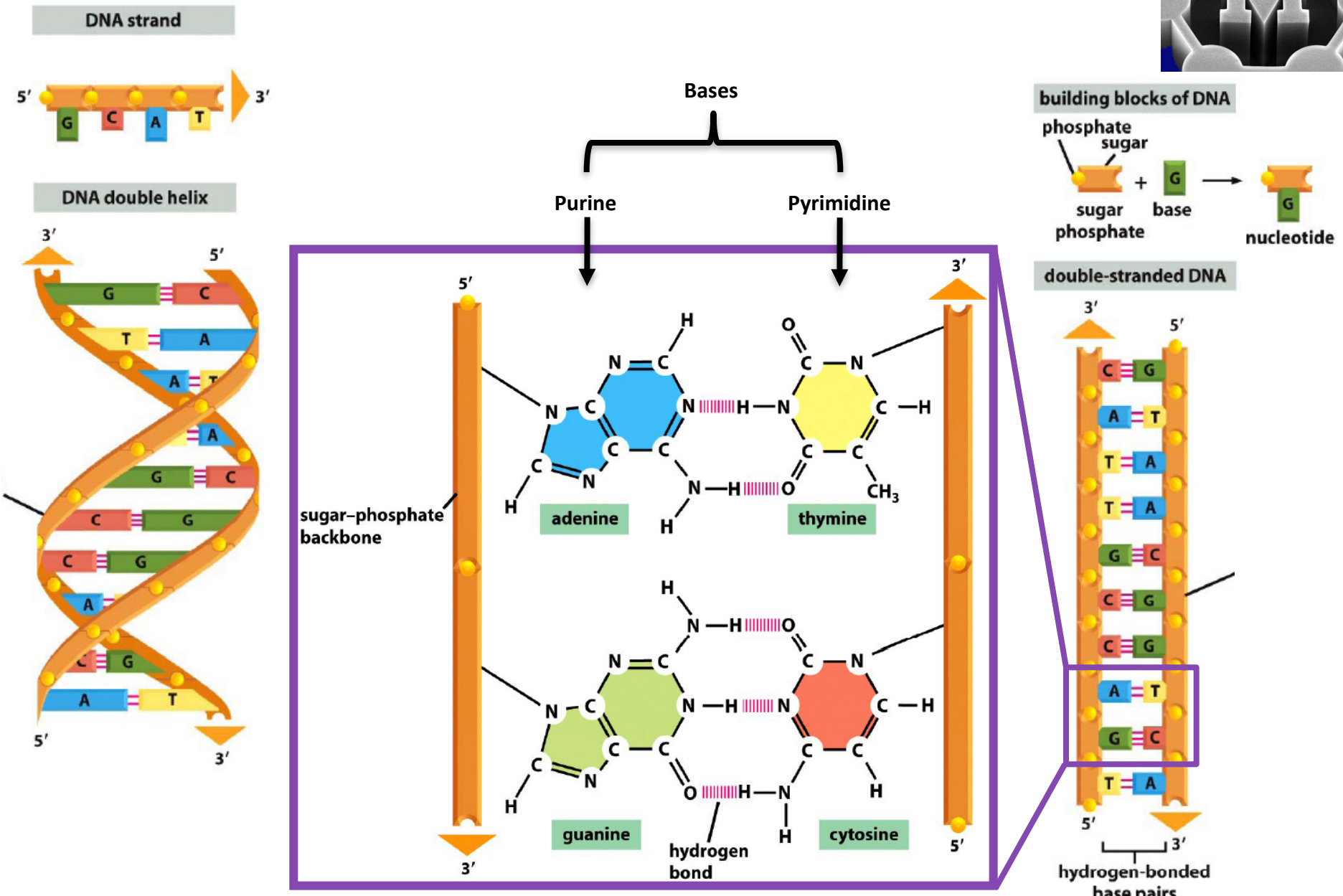

DNA-mediated assembly of Au NPs

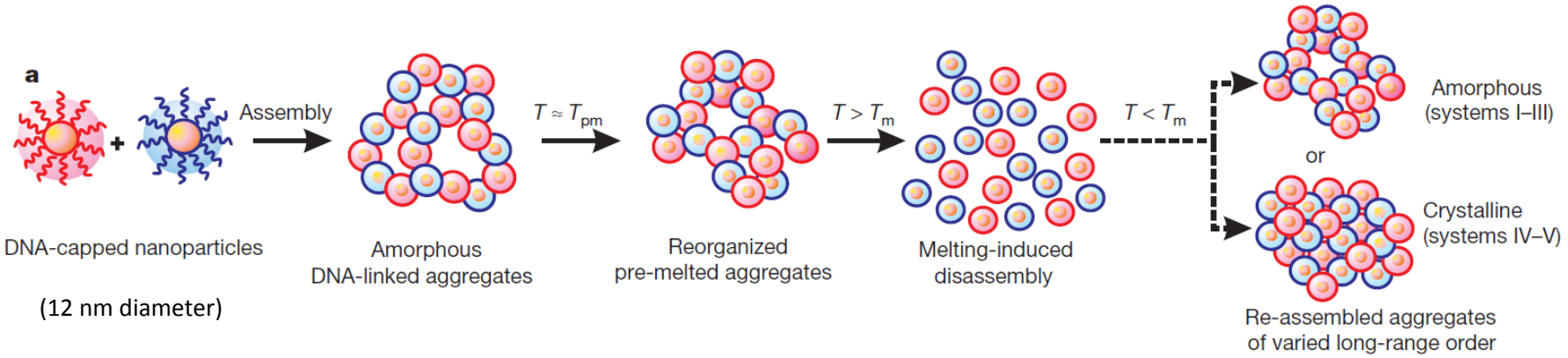

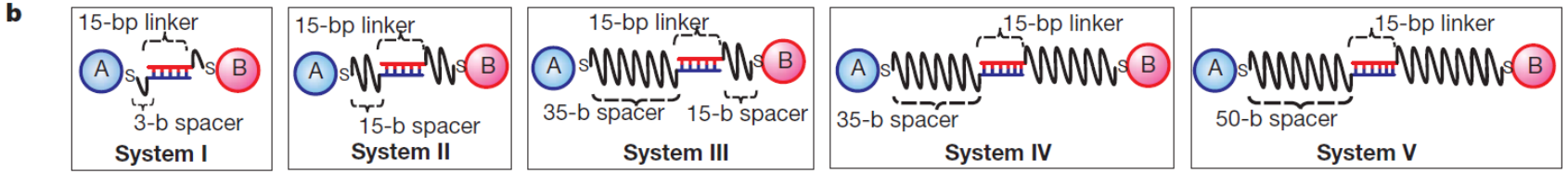

- Attractive potential ➔ Constant (15-bp linker)
- Repulsive potential ➔ Varied (n-b spacer)

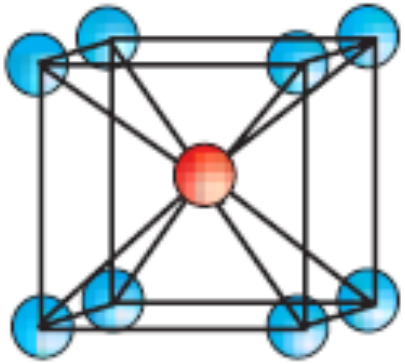

Nykypanchuk *et al.*, *Nature, Vol. 451, No. 31, 2008.*

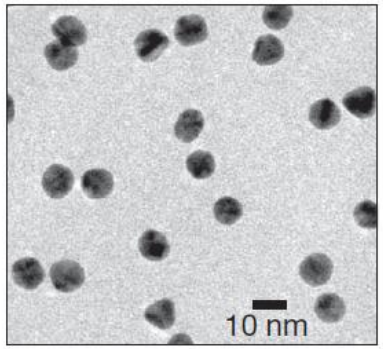

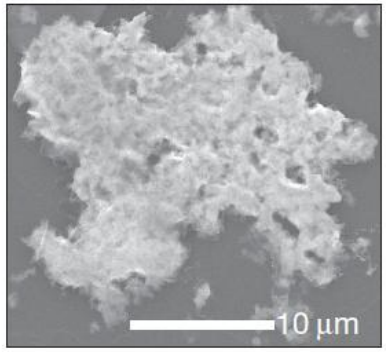

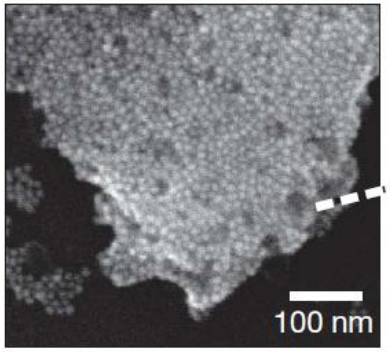

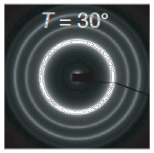

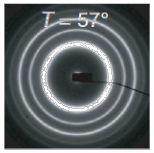

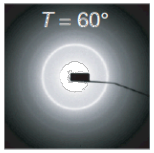

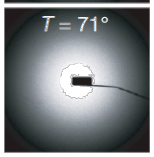

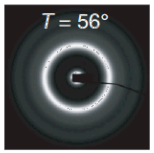

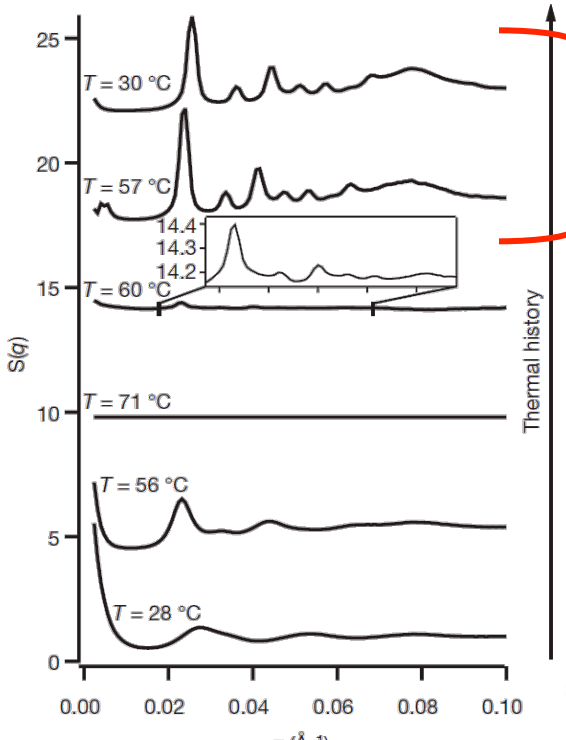

Highly ordered polycrystalline BCC

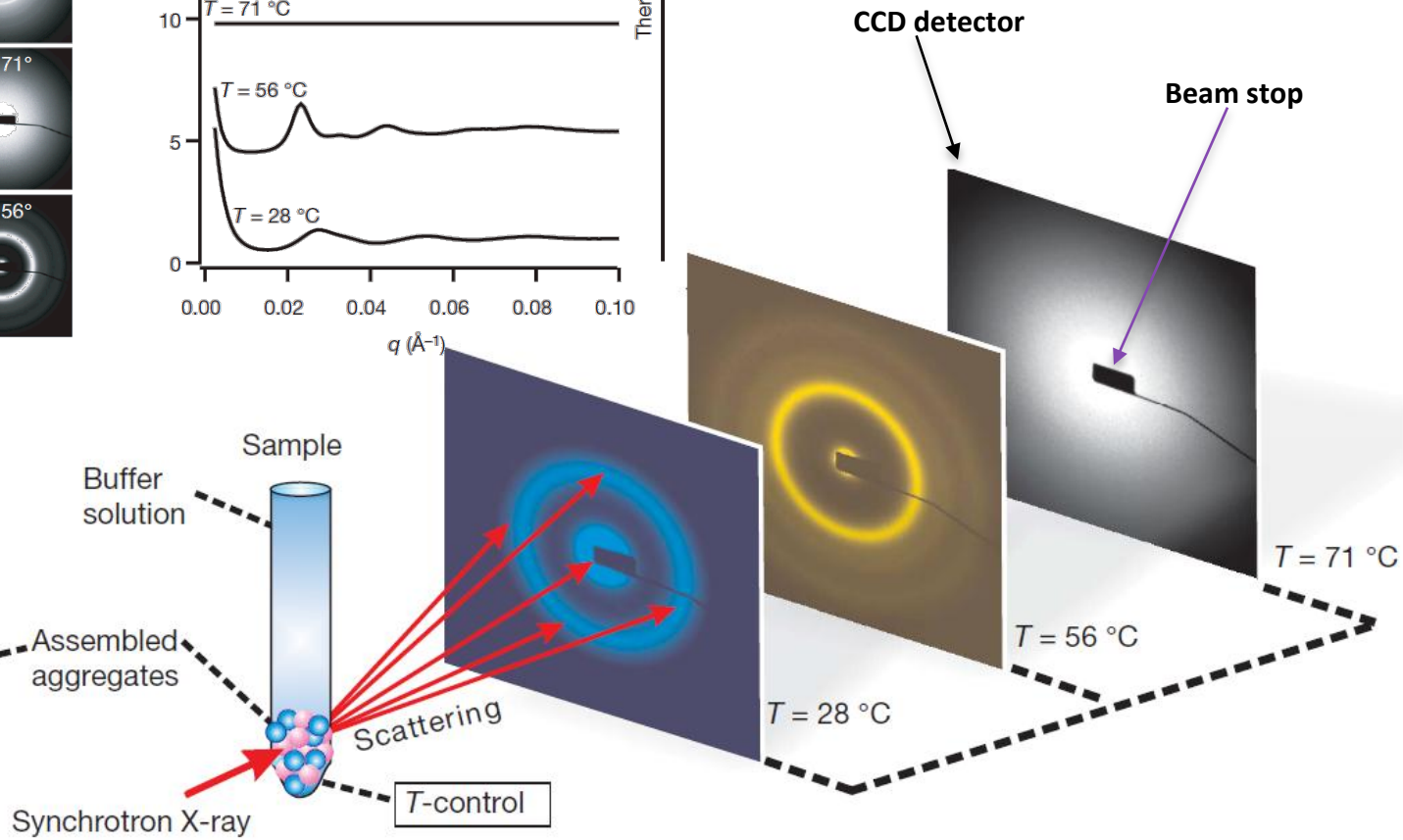

Nykypanchuk *et al.*, *Nature, Vol. 451, No. 31, 2008.*

DNA origami

- Long backbone with hairpin turns
- Short staples bind to specific “patches” of backbone

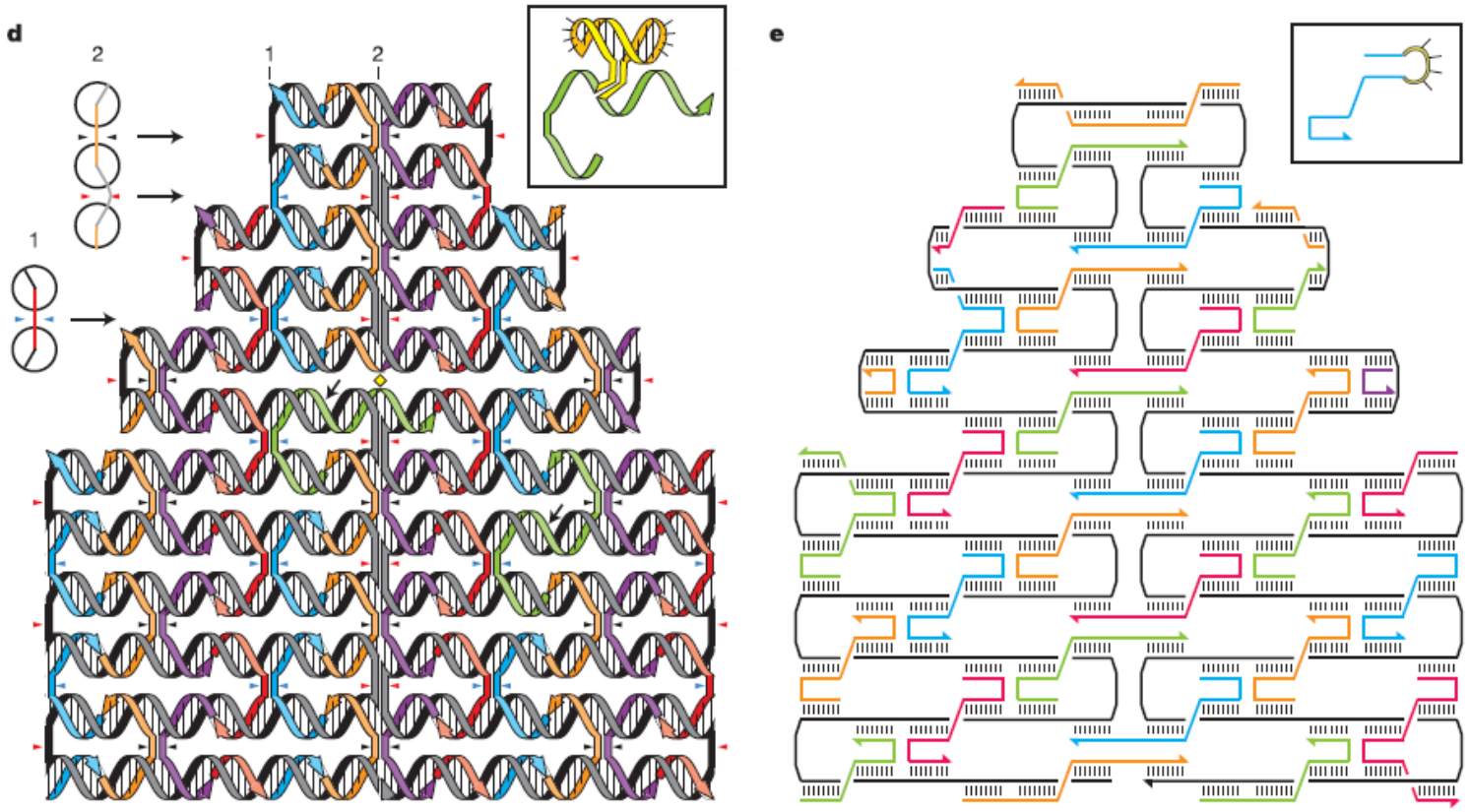

Rothemund, *Nature* 440(16):297-302, 2008.

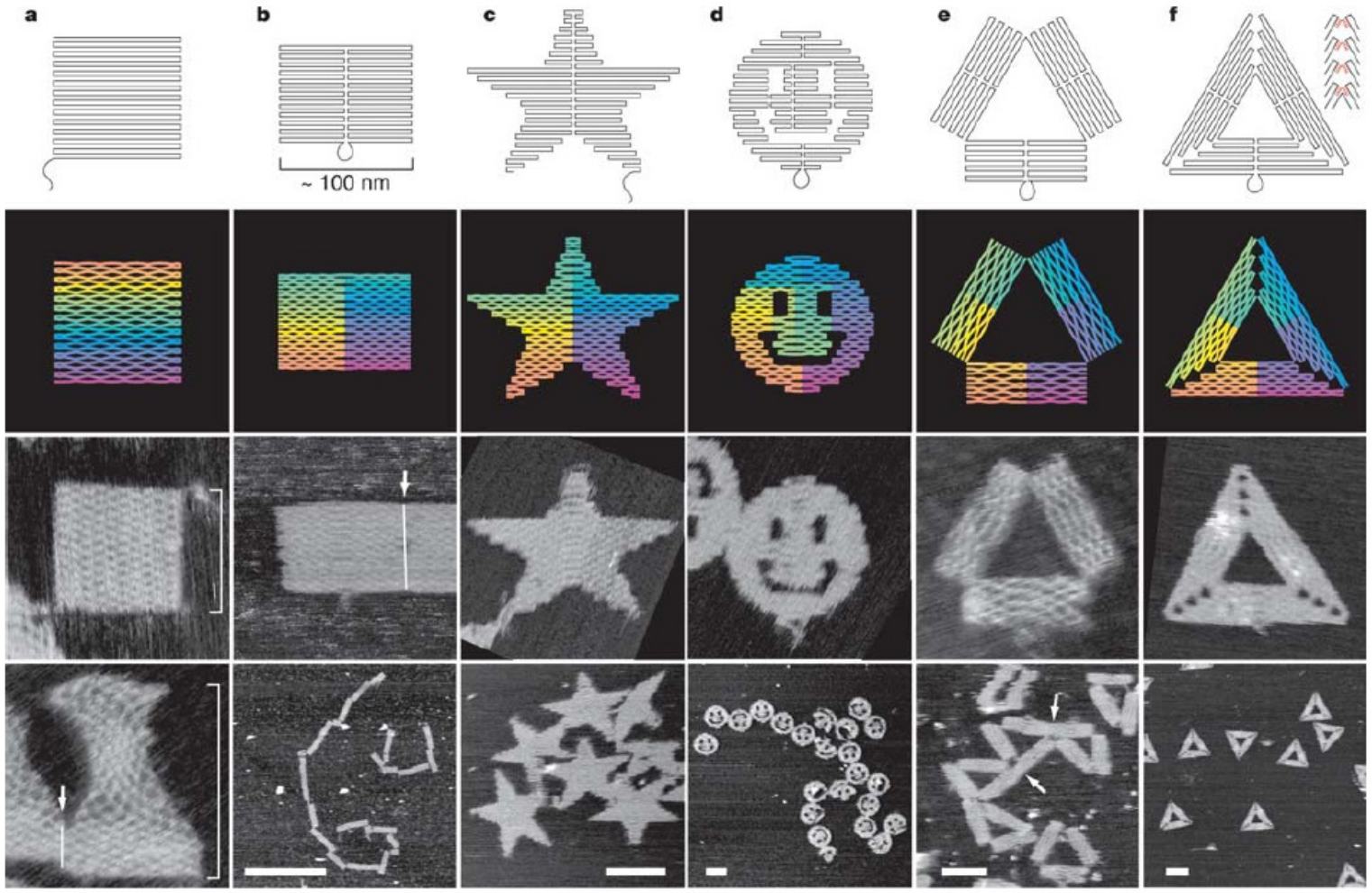

Rothemund, *Nature* 440(16):297-302, 2008.

Docking DNA origami

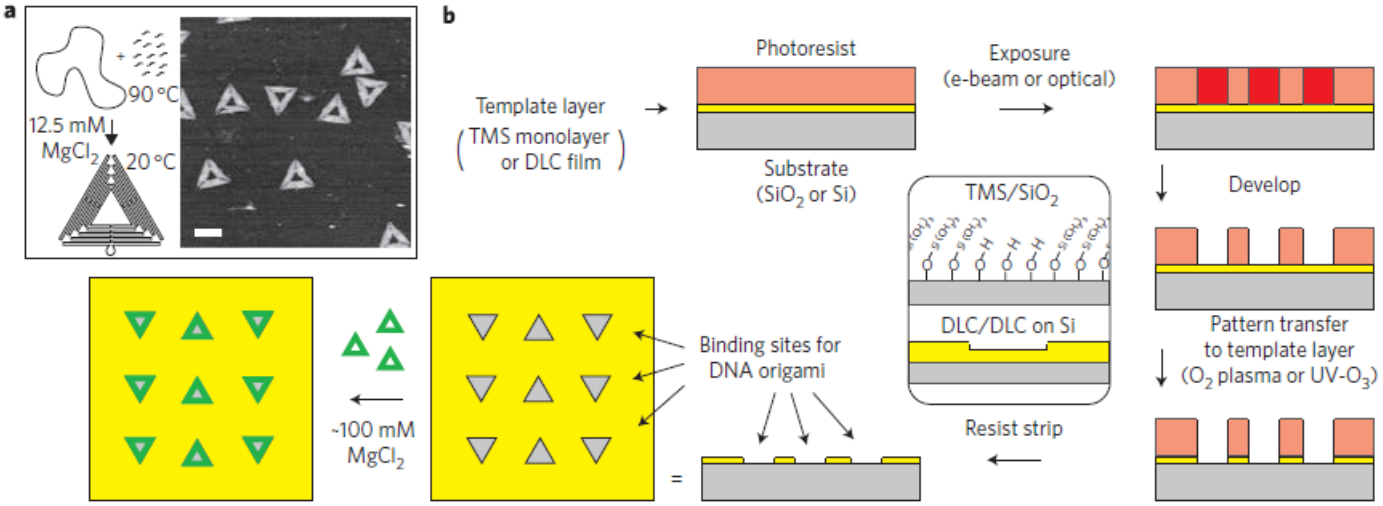

Figure 1 | The problem of random DNA nanostructure deposition and a lithographic scheme for addressing it. a, Synthetic scheme for DNA origami triangles (left) and atomic force microscopy height image (right) showing random deposition on mica. The triangles' edges are ~127 nm; scale bar, 100 nm. **b**, Fabrication of DNA origami binding sites. The inset highlights differentiation of the background and features (background/features) for the trimethylsilyl (TMS) monolayer and diamond-like carbon (DLC) films. Silanol groups occur in oxidized areas of the TMS monolayers. Features etched into the ~10-nm DLC template layer are 0.5–1.5 nm deep. No silicon is exposed; such surfaces have DLC features on a DLC background, and so we refer to them as 'DLC/DLC'.

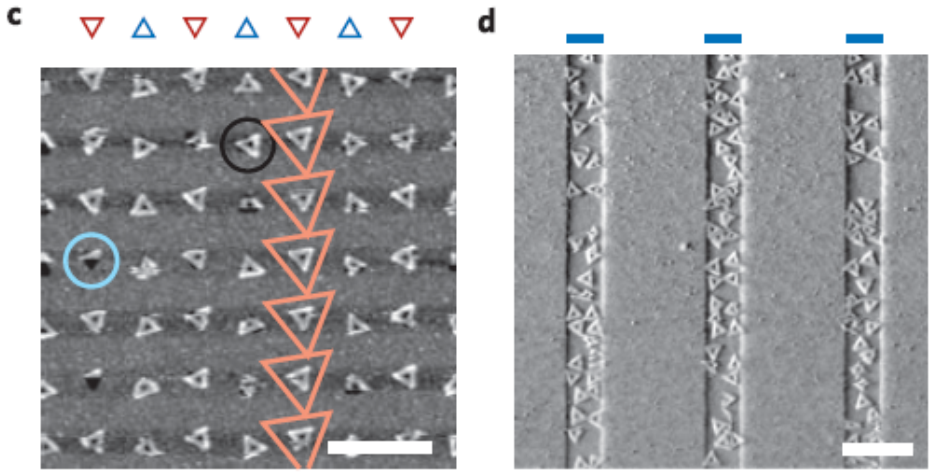

Kershner et al., *Nature Nanotechnology* 2009.